

Component based design model for composite beam to reinforced  
concrete wall moment-resistant joints

Peer-reviewed author version

GOUVEIA HENRIQUES, Jose; Gentili, Filippo; Simões da Silva, Luis Simoes &  
Simões, Rui (2015) Component based design model for composite beam to  
reinforced concrete wall moment-resistant joints. In: Engineering structures, 87, p. 86-104.

DOI: 10.1016/j.engstruct.2014.12.039

Handle: <http://hdl.handle.net/1942/31900>

# Component based design model for composite beam to reinforced concrete wall moment-resistant joints

**J. Henriques<sup>a</sup>, F. Gentili<sup>a</sup>, L. Simões da Silva<sup>a</sup>, R. Simões<sup>a</sup>**

*<sup>a</sup> ISISE, Civil Engineering Department, University of Coimbra, Pinhal de Marrocos, 3030 Coimbra, Portugal*

---

## **Abstract**

The use of the structural systems combining members of different nature, such as reinforced concrete walls with steel/composite beams and columns, presents a competitive solution benefiting from the structural efficiency of each type of member. This paper investigates the behavior of a composite beam to reinforced concrete wall moment-resistant joint configuration. The proposed joint configuration is a simple solution with structural capacity to connect these types of members in a non-seismic region. An experimental campaign was conducted within the work programme of a RFCS research project that demonstrated the structural efficiency of the joint.

An analytical component based design model is proposed. The development of the model was performed with the aid of numerical simulations and experimental results. In the present paper, the calibration and validation of model is first presented for parts of the joint, where only several components are activated, and after the global model is assembled and verified against the experimental results. Subsequently, a parametric study is presented extending the range of validity of the model. Finally, this study shows the need to detail the concrete components appropriately (wall) in order to prevent brittle failure of the joint.

Key-words: Structural steel-to-concrete joints, Behavior of joints, Component method, Moment-rotation curve, Design model

---

## **1. Introduction**

In many cases the use of mixed steel-concrete structures is the most competitive solution. The concept of mixed structure is based on using different materials for different members according to their best structural performance. Clear examples of this practice are the use of reinforced concrete (RC) for foundations staircases/lift cores and steel/composite for columns, slabs and beams. Optimized solutions can be obtained in terms of structural performance, weight of the structure, erection time and therefore cost. A typical example of the efficiency of this practice is the Millennium Tower in Vienna [1].

Besides the aspects of global analysis, when dealing with the design of mixed structures, engineers are faced with two distinct aspects: the design of members and joints and the design of interfaces between different materials. The Eurocodes [2]-[4] appropriately address the first aspect; however, for the latter, when steel/composite members have to be connected to reinforced concrete members, a lack of guidance is evident. Current solutions consist on the development of creative models, defined for particular or exceptional situations, based on methods used for steel and concrete [5]. However, the complexity of such models requires a high level of expertise in three fields: i) steel connections; ii) anchorage in concrete (using fasteners or reinforcement bars); and iii) concrete.

For the design of steel and composite joints, the component method is nowadays a consensual approach, with proven efficiency, that is able to evaluate the nonlinear response of steel/composite joints. This approach, firstly developed for steel joints and later extended to composite joints, is now common practice in Europe. In Eurocode 3 Part 1-8 [6] the method is prescribed and several joint configurations may be analyzed accordingly. In Eurocode 4 Part 1-1 [4] the extension to composite joints is made adding the transmission of forces achieved through the composite slab and the strengthening of several components due to the embedment of steel components in concrete.

The anchorage in concrete is a key part of a steel-to-concrete joint; however, it is not a mainstream task in the activity of “steel” designers. In recent years, considerable research work has been performed in this field. The knowledge on this field is well expressed in several design guides and standards, such as: CEB Design Guide [7], ETAG 001 [8], ACI 318 [9], fib Design Guideline [10], CEN Technical Specifications [11], Eligehausen et al. [12]. The underlying design philosophy is based on capacity design, evaluating the resistance of the anchorage and disregarding its deformation.

Concerning the reinforced concrete part of the joints in a mixed steel-concrete structure, discontinuity regions (D-region) are “generated” in the reinforced concrete member. In such regions, the strain distribution is significantly nonlinear. Due to the inapplicability of truss models for such complex regions, a rational approach has been developed known as strut-and-tie models (STM). This approach simplifies the design with some loss of accuracy; however, it is a preferable methodology when compared to an empirical approach based on detailing, experience and good practice [13]. The use of strut-and-tie models is currently the approach prescribed in Eurocode 2 [2] for the design of reinforced concrete members where a non-linear strain distribution is expected, such as supports, near concentrated loads, etc.

Clearly, the lack of background knowledge is not an issue for an efficient analysis of joints in mixed steel-concrete structures. The main obstacle relies in the absence of unification of the different approaches that can be integrated in design standards and the design practice of engineers. Even if joints between steel and concrete members such as column bases [14] have been addressed in the past, the design approach remained distinct. The concrete part is dealt with independently by the concrete “side”, as

prescribed by the steel code [6]. Furthermore, beam to wall joints, in mixed steel-concrete structures, are completely disregarded.

Recently, an European RFCS (Research Fund for Coal and Steel) research project entitled “InFaSo - New market chances for steel structures by innovative fastening solutions” [15] was devoted to the analysis of joints in mixed steel-concrete structures. At the European level, for such type of joints, this was a first step regarding the development of simplified design models that assemble all active parts, with special emphasis on the anchorage in concrete. As a complement of this research work, at the University of Coimbra, a PhD thesis [16] was developed. In this paper, the study of the behavior of composite beam to reinforced concrete wall joint is presented. The results of the experimental tests and the proposed analytical model are exposed. Given the limited number of tests performed, numerical simulations were performed to complement the analysis and to further support the analytical proposals. The validation and calibration of these numerical simulations has been previously published [17]-[18] and therefore no detailed information about these simulations is herein provided. Finally, a parametric study using the proposed analytical model is presented extending the range of the different parameters influencing the joint response.

The studied joint configuration is illustrated in Fig. 1 and may be divided in two parts: i) upper part, connection between reinforced concrete slab and wall; ii) bottom part, connection between steel beam and reinforced concrete wall. In the upper part, the connection is achieved by extending and anchoring the longitudinal reinforcement bars of the slab (*a*) into the wall. Slab and wall are expected to be concreted in separate stages and therefore, the continuity between these members is only provided by the longitudinal reinforcement bars. In the bottom part, the fastening technology is implemented to connect the steel beam to the reinforced concrete wall. Thus, a steel plate (*b*) is anchored to the reinforced concrete wall using headed anchors (*c*), pre-installation system. The plate is embedded in the concrete wall with aligned external surfaces. Then, on the external face of the plate, a steel bracket (*d*) is welded. A second plate (*e*) is also welded to this steel bracket but it is not aligned in order to create a “nose”. The steel beam with an extended end plate (*f*) sits on the steel bracket, and the extended part of the end plate and steel bracket “nose” perform an interlock connection avoiding the slip of the steel beam out of the steel bracket. A contact plate (*g*) is welded to the extended end plate (*f*), at the level of the beam bottom flange.

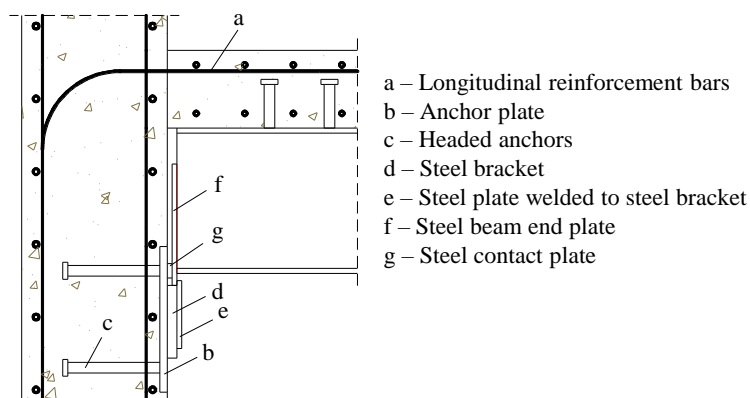


Fig. 1: Composite beam to reinforced concrete wall joint configuration according to the *InFaSo* project report [15]

Finally, it is noted that this joint configuration was developed for application in non-seismic regions and therefore the study was limited to the case of the joint submitted to hogging bending moment.

## 2. Experimental research

### 2.1 Description of the experimental programme

The test programme comprised six tests. Three were performed at the Institute for Structural Design of the University of Stuttgart (USTUTT) and the other three at the Faculty of Civil Engineering of the Czech Technical University in Prague (CTU). The configuration of the reference test specimen consists of a cantilever composite beam supported by a reinforced concrete wall (Fig. 2). The geometry of the test specimens varied within each group of three tests. One specimen had the same geometric properties and therefore was common to both groups. Besides this common test specimen, the variation of geometry differed from one institution to another. In Stuttgart, the variation consisted of the percentage of reinforcement in the slab and the disposition of the shear studs in the composite beam ( $a$  – distance of the first shear stud to the joint face). In Prague, the geometric parameters, thickness of the anchor plate and the steel bracket, were varied. The geometric and material properties within the different test specimens are summarized in Table 1 and Table 2, respectively. The test procedure relied on applying a concentrated load at the free-end of the cantilever beam with a hydraulic jack up to failure. The tests were static monotonic and were performed using displacement control. The reinforced concrete wall was fixed at bottom and top.

In Fig. 3 the test layout is shown. Test results were obtained by monitoring displacements at beam's end, along the beam, on the wall and on the anchor plate; load on the hydraulic jack; crack opening on the composite beam; strains on longitudinal reinforcement inside the composite beam. The interested reader may find more detailed information on the tests in the *InFaSo* project report [15].

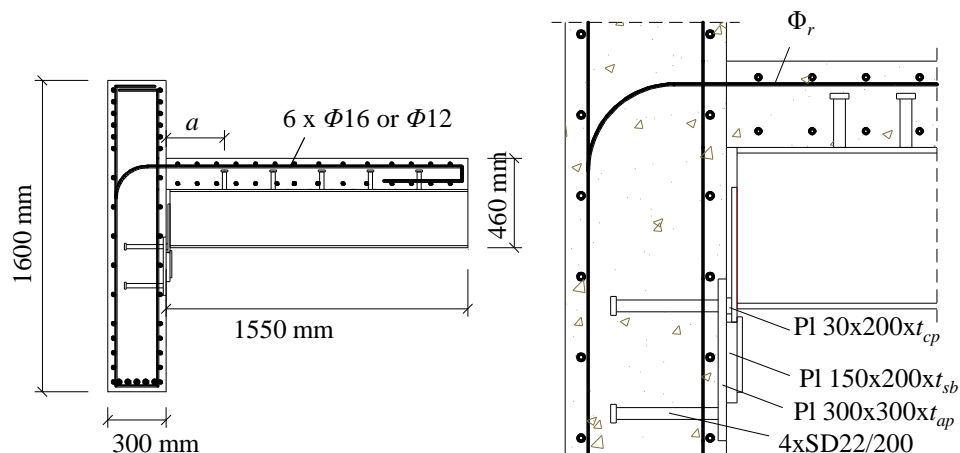


Fig. 2: a) Test specimen's general configuration; b) Joint detail

Table 1: Geometric properties of the experimental tests on composite beam to reinforced concrete wall joint [15]

Test ID	Stuttgart tests			Prague tests		
	SP13	SP14	SP15	P15-20	P15-50	P10-50
$t_{ap}$ [mm]	15	15	15	15	15	10
$t_{sb}$ [mm]	20	20	20	20	50	50
$\Phi_r$ [mm]	16	12	16	16	16	16
$a$ [mm]	500	270	270	270	270	270

Table 2: Mean values of the material properties of the experimental tests on composite beam to reinforced concrete wall joint [15]

Test ID	Concrete Wall [ $f_{ck,cub}$ ] MPa	Concrete Slab [ $f_{ck,cub}$ ] MPa	Steel Long rebars ( $f_y; f_u; \epsilon_y; \epsilon_u$ ) MPa; MPa; %; %	Steel Headed Anchors ( $f_y, f_u$ ) MPa; MPa	Steel Plates ( $f_y, f_u$ ) MPa; MPa	Steel Profile ( $f_y, f_u$ ) MPa; MPa
SP13	73.5	71.3	520; 673.11; 2.62; 73.58	460; 562	427; 553	380; 539
SP14	71.6	66.1	540; 679.27; 3.14; 81.89	Same as SP13	Same as SP13	Same as SP13
SP15	70.3	69.9	Same as SP13	Same as SP13	Same as SP13	Same as SP13
P15-50	83.3	73.0	Same as SP13	Same as SP13	Same as SP13	Same as SP13
P10-50	83.3	73.0	Same as SP13	Same as SP13	Same as SP13	Same as SP13
P15-20	71.4	62.5	Same as SP13	Same as SP13	Same as SP13	Same as SP13



Fig. 3: Test layout [15]

## 2.2 Test results

In all tests, failure occurred by rupture of one of the longitudinal steel reinforcement bars in tension. Consequently, the longitudinal steel reinforcement in tension was the component governing the behavior of the joint. The Prague tests demonstrated that the variations of the anchor plate and steel bracket geometry did not affect significantly the results, leading to similar results for all tests. In contrast, in the Stuttgart tests, the behavior of the joint was completely governed by the longitudinal steel reinforcement. For this reason, only the tests performed in Stuttgart are used hereafter.

Fig. 4 presents the moment-rotation curves. Fig. 5 illustrates a test specimen after failure. A ductile failure is confirmed by the rotation capacity achieved in all tests. The variation of the percentage of reinforcement resulted in a significant variation of the resistance, showing an increase between SP14 and SP13/SP15 of about 80%. In what concerns the effect of the position of the shear studs  $a$ , as observed in Schäfer [19], there is an influence on the deformation capacity of the joint. The comparison between test specimen SP13 and SP15 reveals that higher ultimate rotation is obtained with a higher value of  $a$ . This result is consistent with the experimental observations in Schäfer [19]. For smaller values of  $a$ , the cracks concentrate near the joint face resulting in a smaller elongation length contributing to the joint rotation. Higher slip was observed closer to the joint, and with the increase of the distance to the joint, the slip diminished. Table 3 summarizes the joint mechanical properties observed in the tests.

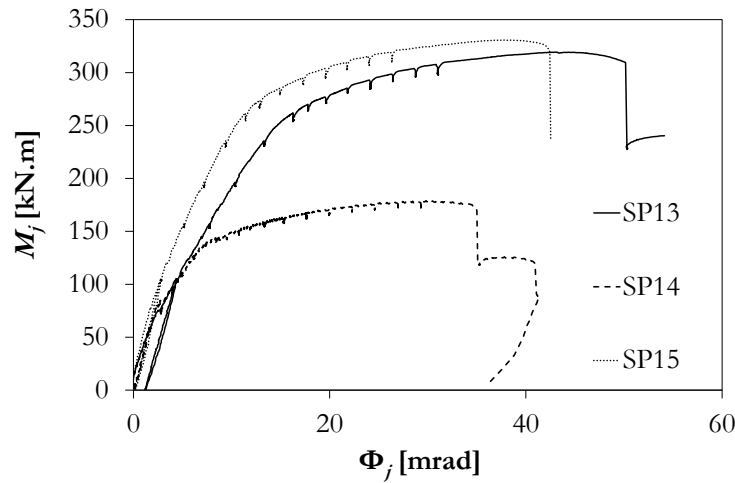


Fig. 4: Joint moment-rotation curves [15]

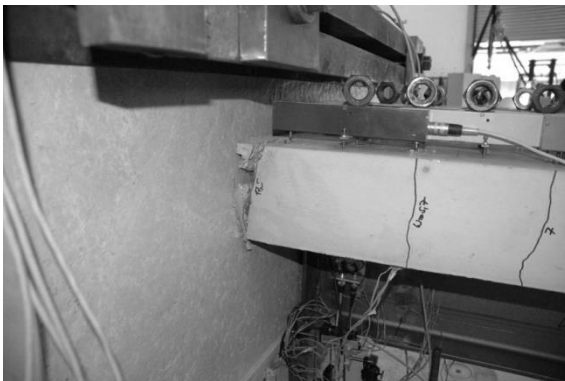


Fig. 5: Test specimen SP14 at failure [15]

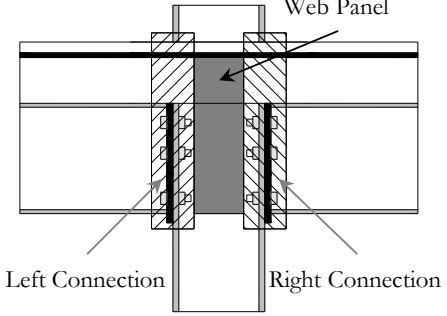
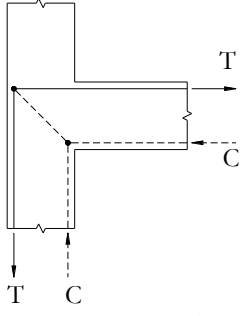
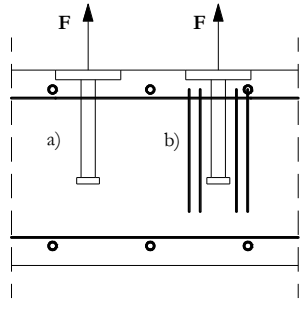
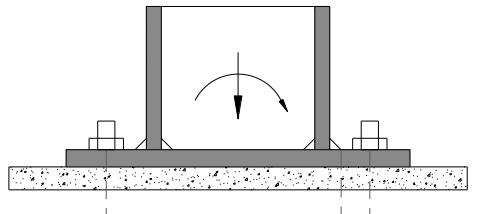
Table 3: Summary of the joint mechanical properties of all tested specimens

	SP13	SP14	SP15
$S_{j,ini}$ [kN.m/rad]	25076.4	32917.9	37390.6
$M_{j,max}$ [kN.m]	319.3	178.9	330.8
$\Phi_{j,u}$ [mrad]	50.2	35.00	42.4

### 3. Background for the design of steel-to-concrete joints

The design of steel-to-concrete joints requires extensive knowledge on steel and composite joints, reinforced concrete joints and anchorage in concrete. A great deal of background information exists and a thorough review and discussion may be found in Henriques [16]. Table 4 summarizes the main approaches required for the design of steel-to-concrete joints. These form the basis of the design model proposed in this paper.

Table 4: Main background for the design of steel-to-concrete joints

Type of Joint/Connection	Background knowledge	Reference
 <p style="text-align: center;">Steel and composite</p>	<p>Component Method Evaluation of components Construction of spring models Assembly of joint components to determine joint properties</p>	<p>[4], [6], [20],[21], [22], [23]</p>
 <p style="text-align: center;">Reinforced concrete joints</p>	<p>STM models Evaluation of struts, ties and nodes resistance</p>	<p>[2], [13], [25], [26], [27], [28]</p>
 <p style="text-align: center;">Anchorage in concrete</p>	<p>Different type of anchorage in concrete Evaluation of the failure modes associated to specific anchor type</p>	<p>[7], [8], [9], [10], [11], [12]</p>
	<p>Column bases models and related components Anchor plate connection models and new advances steel-to-concrete joints (<i>InFaSo</i> research project)</p>	<p>[6], [14], [15], [29], [30]</p>



#### 4. Design model: component base model

##### 4.1 General considerations

In order to extend the method to steel-to-concrete joints, the joint components activated in the selected joint configuration (subject to hogging bending moment) are listed in Table 5 and their positions are shown in Fig. 6. It is noted that the number attributed to the joint components does not follow the usual numbering in Eurocode 3 Part 1-8 [6].

Table 5: List of components

Component ID	Basic joint component	Type
1	Longitudinal steel reinforcement bar in the slab	Tension
2	Slip of composite beam	Tension
3	Beam web and flange	Compression
4	Steel contact plate	Compression
5	Anchor plate in bending under compression	Compression
6	Concrete in compression	Compression
7	Headed anchor in tension	Tension
8	Concrete cone	Tension
9	Pull-out of anchor	Tension
10	Anchor plate in bending under tension	Tension
11	Concrete panel	Tension and Compression
12	Hanger reinforcement	Tension
13	Plate-concrete friction	Vertical Shear
14	Headed anchor in shear	Vertical Shear
15	Concrete pry-out	Vertical Shear

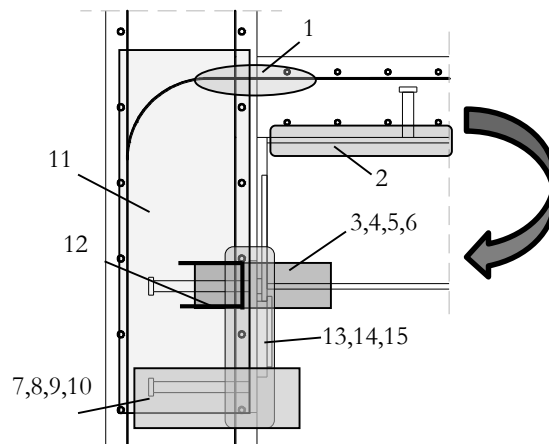


Fig. 6: Location of the joint components

As referred above, this joint configuration was developed for non-seismic regions. Accordingly, the joint was studied for hogging bending moment loading conditions only. In Henriques [16] was shown that the shear load has a residual effect on the joint response and consequently, its effects may be analyzed separately. Thus, for hogging bending moment, the joint can be subdivided in three groups of components, according to their role on the joint behavior: i) anchor plate connection in compression (bottom part of the joint); ii) tension components (upper part of the joint); iii) concrete panel (equilibrium between tension and compression introduced into the wall). In the following sections, the models proposed for each of these parts of the joint are presented. Subsequently, the joint global model is described and validated, through comparison with experimental tests and numerical simulations.

## 4.2 Anchor plate in compression

### 4.2.1 Introduction

The analytical model proposed for the anchor plate was developed considering this connection as an isolated connection subject to similar loading conditions as in the composite beam to reinforced concrete wall joint depicted in Fig. 6. Accordingly, the anchor plate connection is subjected to pure compression and the shear load is neglected, as illustrated in Fig. 7. Analogously to column bases, the problem can be seen as the component plate in bending under compression with headed anchors on the non-loaded side of the plate. In Eurocode 8 Part 1-8 [6], the referred component may be represented by a T-stub in compression, which is a simplified model with practical interest. However, this model cannot take into consideration the effect of the headed anchors on the non-loaded side. Therefore, a more sophisticated modeling of the anchor plate in compression reproducing their effect is proposed, based on the sophisticated model for columns bases proposed in Guisse at al. [29]. Finally, for practical use, a modification of the T-stub in compression is proposed that incorporates the effect of the headed anchors on the non-loaded side.

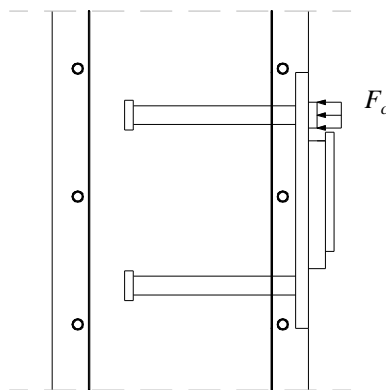


Fig. 7: Anchor plate subject to pure compression

#### 4.2.2 Sophisticated model

Based on numerical analysis [16], [17] and the model for column bases proposed in Guisse et al. [29], a sophisticated mechanical model for the anchor plate connection subject to pure compression was idealized. It is represented in Fig. 8 and considers the following components (Table 5): i) extensional springs for the concrete in compression under the plate (component 6); ii) three rotational springs located at the sections of the plate where significant bending of the plate was numerically observed (components 5 and 10); iii) three extensional springs in the positions of anchor row on the non-loaded side of the connection (components 7 to 9). These springs represent the components activated within the connection. Despite the level of sophistication of the model, it corresponds to a 2D model that neglects the 3D behavior of the connection. The 3D effects in the connection were incorporated in a simplified way in the components (springs) behavior.

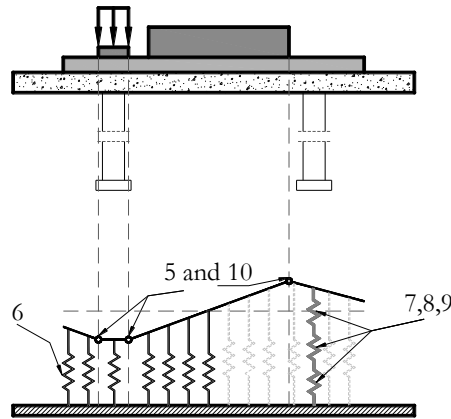


Fig. 8: Spring mechanical model proposed to reproduce the anchor plate connection subject to pure compression

##### a) Concrete in compression (Component 6)

The concrete in compression component depends on the plate-to-concrete contact. For this reason the component is represented by a group of springs. The more springs are used the better the approximation for the identification of the boundary of the no contact section. For the determination of the component properties it is necessary to define the dimension under the plate where stresses are admissible. Fig. 9 illustrates the “effective” dimensions of the plate. It was assumed that the whole length ( $l_{ap}$ ) of the plate may be under compressive stresses. The development of stresses on the farthest edges from the loaded area ( $l_{cp} \times b_{cp}$ ) depends on the flexibility of the plate, which is taken into consideration in the model using the rotational springs. For the width, similarly to the Guisse model [29], two zones are distinguished: i) within the contact plate length ( $l_{cp}$ ); ii) and outside the contact plate length. For the first zone, the concept of equivalent rigid plate was used, requiring the determination of the bearing width “ $c$ ”, as defined in Eurocode 8 Part 1-8 [6] for the T-stub in compression. In the second zone, all the plate width is assumed. It is noted that along the width of the two zones the contact stresses are assumed constant. Finally, the thick dashed lines in Fig. 9 represent the location of the rotational springs.

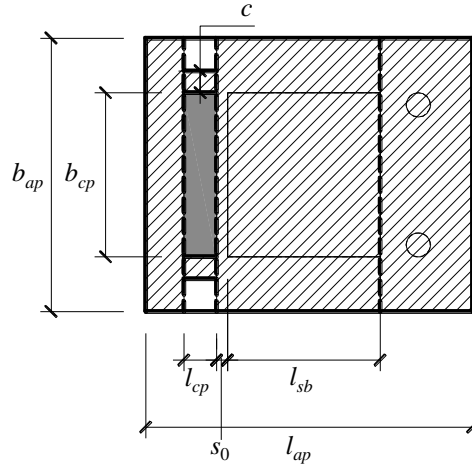


Fig. 9: Effective plate dimensions considered in the sophisticated model for the anchor plate connection subject to pure compression

In order to reproduce the behavior of the concrete in compression the expression proposed by Guisse [29] is used. It is based on a parabolic constitutive stress-strain relation. However, instead of using the characteristic cylinder strength of the concrete ( $f_{ck}$ ), an amplified bearing strength ( $f_j$ ) is considered, because of the beneficial effect of the confinement on the load bearing zone, as in the T-stub in compression model [6]. In this model, the maximum bearing strength of the concrete is achieved at an ultimate strain  $\varepsilon_{cu}$  and followed by a plateau. Here, the concrete is assumed to fail when the ultimate strain ( $\varepsilon_{cu}$ ) is reached. In order to convert the stress-strain curve into a force-deformation curve, the concrete-to-plate contact zone was discretized using a set of springs. Each spring represents an equivalent area of contact ( $A_{ci}$ ) where the stresses are assumed constant. Then, for the deformation of the springs, an equivalent concrete height ( $h_{c,eq}$ ) is determined where the strain is assumed constant. The resulting force-deformation relation is expressed in eq. (1). According to the numerical study presented in Henriques [16], the equivalent concrete height ( $h_{c,eq}$ ), which governs the deformability of the component, may be given by eq. (2).

$$F_i = \left[ \frac{f_j - E_c \varepsilon_{cu}}{\varepsilon_{cu}^2} \left( \frac{\delta_i}{h_{c,eq}} \right)^2 + E_c \left( \frac{\delta_i}{h_{c,eq}} \right) \right] A_{ci} \quad (1)$$

$$h_{c,eq} = 12.13 h_c^{0.235} t_{ap}^{0.485} \quad (2)$$

where  $F_i$  is the force in the spring  $i$  of equivalent area of concrete-plate contact ( $A_{ci}$ ),  $E_c$  is the Young's modulus of the concrete,  $\delta_i$  is the elongation of the spring  $i$ ,  $h_c$  is the concrete member thickness and  $t_{ap}$  is the anchor plate thickness.

b) Anchorage in tension (Components 7, 8, 9)

The anchorage in tension comprises the contribution of three components: i) tensile failure of the steel anchors; ii) concrete cone failure; iii) pull-out failure. The analytical characterization of the behavior of these three individual components is summarized in Table 6. It includes new developments from the research project InFaSo [15]. Subsequently, the behavior of the anchorage in tension is determined from the assembly of the components, described in Table 6. The behavior of the individual components and the resulting equivalent component is illustrated in Fig. 10 using the mechanical and geometrical properties of the experimental tests presented above [15].

Table 6: Characterization and assembly of components for the anchorage in concrete

Component	Model		Eq.
Steel failure of anchor shaft	R	$N_{s,k} = A_s f_{yk}$ $N_{us,k} = A_s f_{uk}$	(3)
	D	$K_{s,ini} = \frac{E_s A_s}{l_{a,s}}$	(4)
Concrete cone failure	R	$N_{uc,k} = \frac{A_{c,N}}{A_{c,N}^0} \Psi_{s,N} \Psi_{ec,N} \Psi_{m,N} \Psi_{re,N} \Psi_{ucr,N} N_{uc,k}^0$	(5)
	D	$\delta_c = 0 \rightarrow N = N_{u,c}$ $\delta_c > 0 \rightarrow N = N_{u,c} + \delta_c k_c$ $k_c = \alpha_c \sqrt{h_{ef}} \sqrt{f_{cc,200}} \frac{A_{c,N}}{A_{c,N}^0}$ $\alpha_c = -537$	(6)
Pull-out failure	R	$N_{p,k} = p_k A_h$	(7)
	D	$\delta_{pl} = \alpha_p \frac{k_a k_A}{C_1} \left( \frac{N}{A_h f_{cc,200} n} \right)^2$ <p><math>c_1 = 300</math> for headed studs in un-cracked concrete  <math>c_1 = 600</math> for headed studs in cracked concrete</p> $a_a = 0,5(d_h - d)$ $k_a = \sqrt{5/a_a} \geq 1$ $k_A = 0.5 \sqrt{d^2 + m(d_h^2 - d^2)} - 0.5d_h$	(8)
Assembly	R	$F_{a,max} = \text{Min}(N_{us,k}; N_{p,k}; N_{uc,K})$	(9)
	D	$\delta_a = \sum \delta_i(F_a)$	(10)

\*R – Resistance; D - Deformation

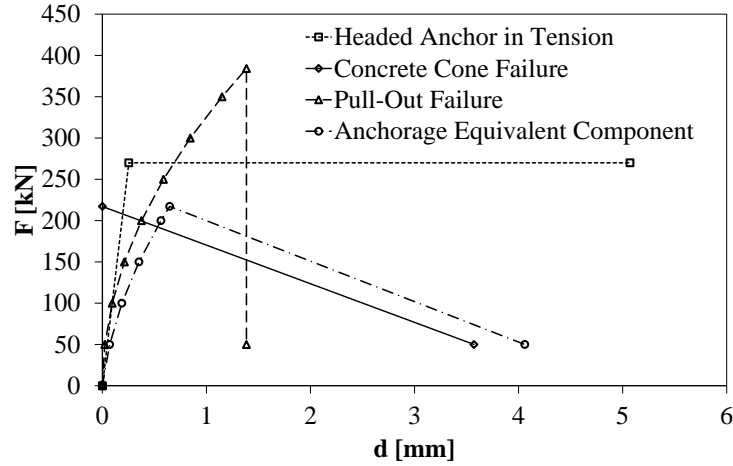


Fig. 10: Force-deformation curve characterizing the behavior of the components activated in anchorage subject to tension

c) Plate in bending under compression and tension (Components 5 and 10)

The behavior of the plate in bending component is derived from the moment-rotation curve of a rectangular cross-section in bending. The total width of the plate is considered to contribute to the section resistance. No hardening is assumed and therefore the maximum resistance is limited to the yield strength ( $f_y$ ) of the steel plate. Accordingly, the maximum bending moment corresponds to the complete yielding of the cross-section. The elastic resistance, plastic resistance and cross-section rotation (curvature), before complete yielding, are determined according to eqs. (11) to (13), respectively, where  $x$  denotes the distance between the opposite steel fibers achieving the yield strain ( $\varepsilon_y$ ). These properties are subsequently assigned to the rotational springs representing components 5 and 10.

$$M_y = \frac{f_y b_{ap} t_{ap}^2}{6} \quad (11)$$

$$M_{pl} = \frac{f_y b_{ap} t_{ap}^2}{4} \quad (12)$$

$$\Phi = \frac{\varepsilon_y}{x} \quad (13)$$

d) Model assembly

The component model for the anchor plate connection in compression is illustrated in Fig. 11 and the assembly procedure follows the formulation proposed in Guisse et al. [29]. The following assumptions apply:

- Forces and displacements are positive downwards while rotations are positive in the anticlockwise direction;
- Four zones are identified and delimited by the edges of the anchor plate and the rotational springs;

- Four degrees of freedom are considered:  $u$ , vertical displacements;  $\alpha_1$ , rotation of the bar in zone 1;  $\alpha_2$ , rotation of the bar in zone 3;  $\alpha_3$ , rotation of the bar in zone 4;
- Bar in zone 2 is assumed to remain in the horizontal position (assumption of constant deformations in the concrete within the contact plate length ( $l_{cp}$ ) as observed numerically);
- The origin of the ( $x$ ) axis is located at the middle of the contact plate length ( $l_{cp}$ ).

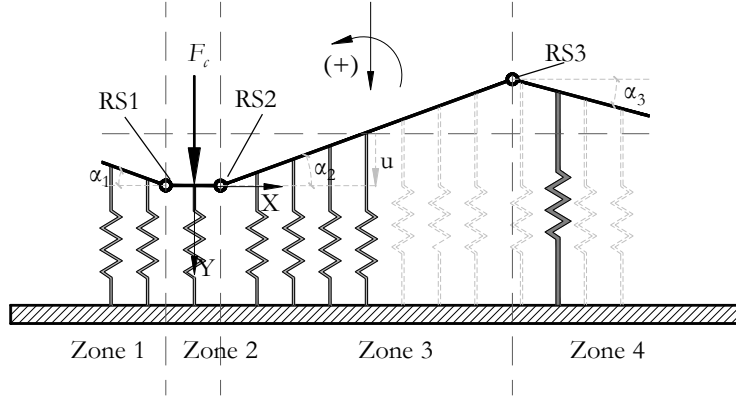


Fig. 11: Schematic representation of the model for the anchor plate in compression

The assumed displacement field may be expressed as follows [16].

$$\begin{aligned}
 \text{Zone 1} \quad u(x) &= u + \alpha_1 \left( x + \frac{l_{cp}}{2} \right) \\
 \text{Zone 2} \quad u(x) &= u \\
 \text{Zone 3} \quad u(x) &= u - \alpha_2 \left( x - \frac{l_{cp}}{2} \right) \\
 \text{Zone 4} \quad u(x) &= u - \alpha_2 (s_0 + l_{sb}) - \alpha_3 \left( x - \left( s_0 + l_{sb} + \frac{l_{cp}}{2} \right) \right)
 \end{aligned} \tag{14}$$

where  $x$  is the position of each spring,  $l_{cp}$ ,  $s_0$  and  $l_{sb}$  are geometrical dimensions of the anchor plate connection as defined in Fig. 9. Eq. (15) describes the resulting vertical and rotational equilibrium equations [16], where  $F_c$  and  $M_i$  represent the external loading (note that  $M_i$  is zero in the present case). Due to the non-linearity of several components, as concrete in compression, pull-out failure and plate in bending, the problem needs to be solved using an iterative procedure. The Newton-Raphson method was adopted.

$$\begin{bmatrix} k_{11} & k_{12} & k_{13} & k_{14} \\ k_{21} & k_{22} & 0 & 0 \\ k_{31} & 0 & k_{33} & k_{34} \\ k_{41} & 0 & k_{43} & k_{44} \end{bmatrix} \begin{bmatrix} \Delta u \\ \Delta \alpha_1 \\ \Delta \alpha_2 \\ \Delta \alpha_3 \end{bmatrix} = \begin{bmatrix} \Delta F_c \\ \Delta M_1 \\ \Delta M_2 \\ \Delta M_3 \end{bmatrix} \quad (15)$$

with

$$\begin{aligned} k_{11} &= \sum k_{z1} + \sum k_{z2} + \sum k_{z3} + \sum k_{z4} \\ k_{12} &= k_{21} = \sum k_{z1} \left( x_{z1} + \frac{l_{cp}}{2} \right) \\ k_{13} &= k_{31} = - \sum k_{z3} \left( x_{z3} - \frac{l_{cp}}{2} \right) - \sum k_{z4} (s_0 + l_{sB}) \\ k_{14} &= k_{41} = - \sum k_{z4} \left[ x_{z4} - \left( s_0 + l_{sB} + \frac{l_{cp}}{2} \right) \right] \\ k_{22} &= \sum k_{z1} \left( x_{z1} + \frac{l_{cp}}{2} \right)^2 + k_{RS1} \alpha_1 \\ k_{23} &= k_{32} = 0 \\ k_{24} &= k_{42} = 0 \\ k_{33} &= \sum k_{z3} \left( x_{z3} - \frac{l_{cp}}{2} \right)^2 + k_{RS2} \alpha_2 + \sum k_{z4} (s_0 + l_{sB})^2 + k_{RS3} \alpha_3 \\ k_{34} &= k_{43} = \sum k_{z4} \left[ x_{z4} - \left( s_0 + l_{sB} + \frac{l_{cp}}{2} \right) \right] (s_0 + l_{sB}) - k_{RS3} \alpha_3 \\ k_{44} &= \sum k_{z4} \left[ x_{z4} - \left( s_0 + l_{sB} + \frac{l_{cp}}{2} \right) \right]^2 + k_{RS3} \alpha_3 \end{aligned}$$

where  $k_{zi}$  represents the stiffness of the extensional springs,  $x_{zi}$  is the position in relation to the referential defined above and  $k_{RSi}$  represents the stiffness of the rotational springs (the tangential stiffness is obtained from the component behavior according to the respective load-deformation behavior).

#### 4.2.3 Simplified model

Noting the similarities between the anchor plate in compression and column bases, specifically in the compression zone, an adaptation of the T-stub in compression Eurocode 3 Part 1-8 [6] is proposed and presented hereafter.

##### a) Direct modifications

The T-stub in compression resistance model was developed regarding its application to column bases where the installation conditions may differ from the anchor plate, namely



the use of grout that is not expected in the latter. Consequently, the foundation joint material coefficient ( $\beta_j$ ), used to determine the concrete bearing strength, is set to 1. This coefficient should be smaller when the use of grout is considered. Thus, an increase of the concrete bearing strength is obtained and consequently of the resistance of the component. This assumption is consistent with results by Weynand et al. [31] that refers ratios between the experiments and calculations ranging from 1.4 to 2.5.

Similarly, for the initial stiffness, the influence of the grout is corrected. As described in Steenhuis et al. [32] and Weynand [31], the stiffness coefficient currently specified in Eurocode 3 Part 1-8 [6] implicitly includes a reduction factor of 1.5 for the quality of the concrete surface and the grout layer influence. Neglecting this reduction factor, the stiffness coefficient is rewritten as follows.

$$k'_{T-stub} = \frac{E_c \sqrt{b_{eff} l_{eff}}}{0.85E} \quad (16)$$

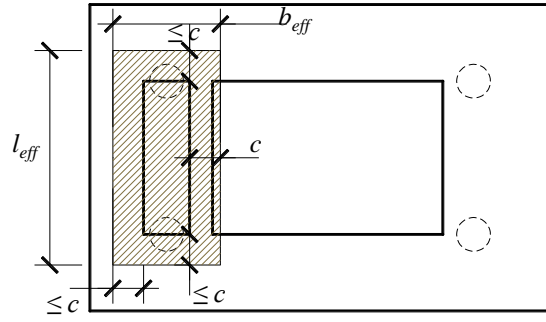
where  $b_{eff}$  and  $l_{eff}$  are the dimensions of the effective T-stub in compression contributing to the initial stiffness and  $E_c$  and  $E$  are the Young's Modulus of concrete and steel, respectively.

b) New proposal for the equivalent rigid plate to determine the component resistance

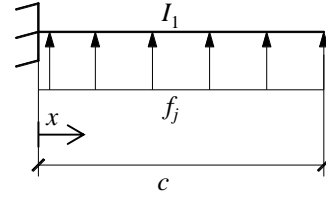
In the resistance model for the T-stub in compression an equivalent rigid plate dimension under uniform concrete bearing stresses ( $f_j$ ) is assumed. The key parameter of the model is the bearing width of the plate  $c$  (Fig. 12a). The latter is obtained calculating a cantilever beam (Fig. 12b) with cross-section properties equivalent to the anchor plate ( $h = t_{ap}$ ;  $b = 1$ ). The value of  $c$  is then obtained by equating the bending moment of this cantilever beam to the yielding of the edge fibers ( $f_y t_{ap}^2 / 6$ ) at the support cross-section. However, the process is iterative, as the bearing strength of the concrete ( $f_j$ ) depends on the bearing width  $c$ . In the anchor plate under study, this model is valid in all directions except on the non-loaded side (side where anchors are activated in tension). Thus, a new bearing width  $c'$  (Fig. 12c) is proposed, determined according to the structural system illustrated in Fig. 12d.

Although the beam in Fig. 12d could be solved by any structural analysis method, the non-uniform cross-section and the uncertainty in the load application length lead to an excessively complex expression for practical use.

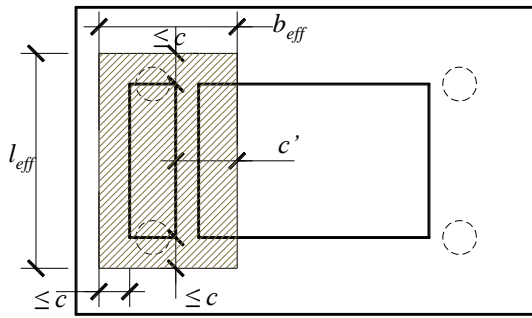
Based on numerical calibration, eq. (17) was adopted as a reasonable approximation of the new bearing width ( $c'$ ) [16].



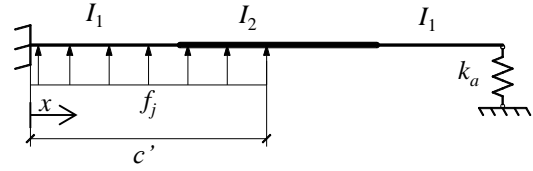
a) Equivalent rigid plate dimensions according to current model



b) Cantilever beam to determine the bearing width (c)



c) Proposal for equivalent plate dimension for the anchor plate



d) Structural system to determine the new bearing width (c')

Fig. 12: Model to determine the concrete in compression resistance using the T-stub model

$$c' = \chi c^\alpha \quad (17)$$

with

$$\alpha = -0.0003f_j + 1.0257$$

$$\chi = \beta\gamma\delta\varepsilon\zeta\eta$$

$$\beta = 1.775f_j^{0.053}$$

$$\gamma = 0.460f_y^{0.135}$$

$$\delta = 572.12 \left( p_1 - \frac{l_{cp}}{2} \right)^{1.203}$$

$$\varepsilon = 0.102l_{sB}^{0.470}$$

$$\zeta = 0.377t_{sB}^{0.2893}$$

$$\eta = -0.0002t_{ap}^2 + 0.0093t_{ap} + 0.937$$

where  $f_j$  is the concrete bearing strength;  $f_y$  is the steel plate yield strength,  $(p_1 - l_{cp})$  is the distance of the non-load side anchors to the contact plate,  $l_{sB}$  is the length of the steel

bracket,  $t_{cB}$  is the thickness of the steel bracket and  $t_{ap}$  is the thickness of the anchor plate.

c) Correction of the bearing width for the stiffness of the component

The stiffness model of T-stub in compression is also based on similar interaction between the concrete and the base plate, as assumed for the resistance. With this model the initial stiffness of the component is estimated. The numerical models [16] used to validate the modifications on the resistance model showed that the initial stiffness of the component is not affected by the presence of the anchors on the non-loaded side of the plate. Therefore, no specific modification for the stiffness model is proposed. However, using the theoretical stiffness model described in Steenhuis et al. [32] and for the loaded dimensions,  $l_{cp}$  and  $b_{cp}$ , from 20 mm to 40 mm and 100 mm to 200 mm, respectively, a new approximation for the bearing width ( $c$ ) was obtained [16], given by eq. (18).

$$c = 1.4t_{ap} \quad (18)$$

#### 4.2.4 Validation and calibration of the model

The process of validation and calibration of the proposed models was performed by comparison with numerical models [16]. A parametric study was performed, described in Table 7.

Table 7: Variables and range of values considered in the parametric study

$t_{ap}$ [mm]	$l_{cp}$ [mm]	$b_{cp}$ [mm]	$l_{sb}$ [mm]	$f_y$ [N/mm <sup>2</sup> ]	$f_{cm}$ [N/mm <sup>2</sup> ]
10	20	100	105	235	24
15	30	150	140	355	45
20	40	200	175	460	68

The calibration of the model, described in detail in Henriques [16], comprised the following aspects:

- Application of a factor  $\alpha_{SR}$  to the rotational springs of the sophisticated model to account for the 3D behavior of the plate. The values found for the factor  $\alpha_{RS1-2}$  and  $\alpha_{RS3}$  were 0.05 and 0.01, respectively.
- Correction factor [16] to determine the concrete bearing strength ( $f_j$ ), which for high concrete grade showed deviations. A factor ( $\alpha_{fcm}$ ) function of the mean concrete strength is then applied. This factor is calculated as follows and applied to both type of models, sophisticated and simplified.

$$\alpha_{fcm} = 6.83f_{cm}^{-0.62} \quad (19)$$

The result of the application of the analytical model is compared with the numerical models in Fig. 13. The numerical simulations have been previously validated in [17]. Only the results considering the variation of the concrete strength are presented, as this was the variable that required a calibration of the model. The sophisticated model presents an excellent agreement. Concerning the simplified model, good agreement is obtained for the stiffness, while conservative results are noted for resistance.

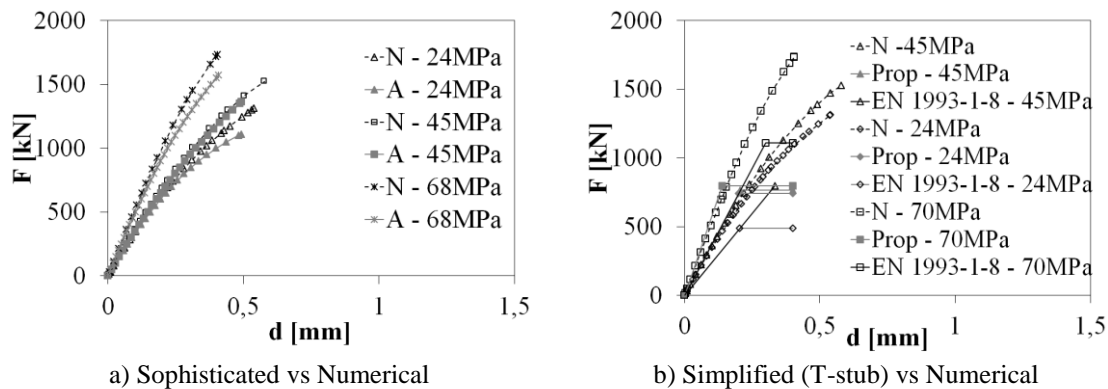


Fig. 13: Comparison between numerical and analytical results: influence of the concrete strength ( $f_{cm}$ )

### 4.3 Tension components

#### 4.3.1 Longitudinal reinforcement in tension

The application of the component method to composite joints assumes each layer of longitudinal reinforcement bars as additional bolt rows. According to Eurocode 4 [4], the longitudinal steel reinforcement bar may be stressed to its design yield strength. It is assumed that all the reinforcement within the effective width of the concrete flange is used to transfer forces. Fig. 14 illustrates the analytical models available [4], [24] to determine the force-deformation response of the component. The code approach is conservative, as it limits the resistance to the yield strength of the steel reinforcement bars. In addition, it does not provide any procedure to evaluate the ultimate deformation capacity. Though, if reinforcement bars class C are used, it may be assumed that sufficient deformation capacity to redistribute the load is available in the case of more than one layer [33]. Regarding the deformation, both models require the definition of the elongation length. In the case of the code approach, this value is constant as it only considers the elastic range. Thus, analogously to the code provisions for single-sided composite joints, the dimension  $h$  involved in determination of the components stiffness coefficient ( $k_{sr}$ ) is assumed, as represented in Fig. 15. Without sufficient experimental data to derive another value, the coefficient 3.6 is kept. In the model proposed in ECCS publication, two parts of longitudinal reinforcement are distinguished in the deformation model: one inside the wall and one inside the slab. The definition of these parts may be found in ECCS Publication n°109 [24].

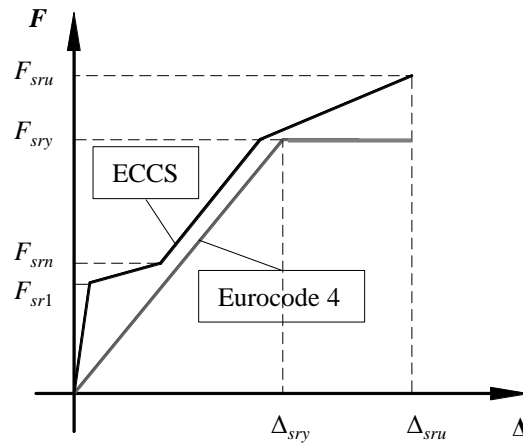


Fig. 14: Force-deformation behavior of the longitudinal steel reinforcement bar in tension

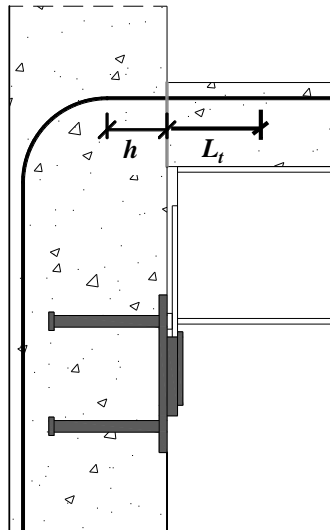


Fig. 15: Definition of dimension  $h$  for the elongation length of the joint component longitudinal steel reinforcement bar in the wall

#### 4.3.2 Slip of the composite beam

The slip of the composite beam is not directly related to the resistance of the joint, although the level of interaction between concrete slab and steel beam defines the maximum load acting on the longitudinal reinforcement bar. In Eurocode 4 [4], the slip of composite beam component is not evaluated in terms of resistance. The level of interaction is considered on the resistance of the composite beam. Concerning the deformation of the joint, in Anderson & Najafi [34] it is demonstrated that the shear connection flexibility could not be excluded from the connection stiffness derivation. Non-negligible influence of the slip between concrete slab and the steel beam on the joint rotation was also observed numerically in Aribert [35]. In Eurocode 4 [4], the influence of the slip of composite beam is taken into account affecting the stiffness coefficient of the longitudinal reinforcement ( $k_{sr}$ )

According to Aribert [35], the slip resistance may be obtained from the level of interaction determined as prescribed in Eurocode 4 [4].

In what concerns the deformation of the component, either the shear load distribution is uniform along the beam and the deformation capacity is then limited by the shear stud with lowest deformation capacity, leading to (Ahmed & Nethercot [36]):

$$k_{slip} = Nk_{sc} \quad (20)$$

or the shear load distribution is non-uniform along the beam and the deformation capacity of the component is then limited by the deformation capacity of the first loaded shear connector [34], yielding:

$$\Delta_{slip} = \left( \frac{F_{slip}}{P_{RK}} \right) \left( \frac{P_{RK}}{k_{sc}} \right) = \frac{F_{slip}}{k_{sc}} \leq \delta_{u,ISC} \quad (21)$$

The model expressed in eq. (20) is stiffer, as all the shear studs contribute to the stiffness of the shear connection, while the latter assumes the stiffness is provided only by one shear stud at the time. In the latter model, a plastic distribution of the interaction load can only be obtained if ductile studs are used. As expressed in eqs. (20) and (21), these are dependent of the stiffness of one shear connector ( $k_{sc}$ ). The range of variation of this parameter is considerable. According to Ahmed & Nethercot [36] it varies between 110 kN/mm and 350 kN/mm. In the code [4] the value of 100 kN/mm is suggested for 19 mm diameter headed stud.

In the case of the composite beam to reinforced concrete wall joint tested in the *InFaSo* project Report [15], the appropriate deformation model is the one expressed in eq. (20). The model was applied to the test specimens in the *InFaSo* project [15]. Initially, as no specific tests on the shear connection were performed, the shear stiffness of one stud was assumed equal to 100 kN/mm. Then, a shear stiffness was determined using the slip observed in the tests. Table 8 presents the results of these calculations. The stiffness of one shear connector calculated with the slip measured in the tests shows that the value of 100 kN/mm is acceptable for this joint.

Table 8: Results of the application of the deformation model for slip of the composite beam component

	<b>Test 1</b>	<b>Test 3</b>
$k_{sc} = 100 \text{ kN/mm}$	$\Delta_{slip} = 0.870 \text{ mm}$	$\Delta_{slip} = 0.898 \text{ mm}$
	$k_{sc}^{calc} = 106.36 \text{ kN/mm}$	$k_{sc}^{calc} = 118.97 \text{ kN/mm}$

#### 4.4 Concrete panel

##### 4.4.1 Introduction

The analytical model for the concrete panel is based on STM and follows the numerical study detailed in Henriques [16]. The numerical study of the concrete panel [16]

identified the main flow of compression stresses between the bend of the longitudinal reinforcement bar and the anchor plate connection, leading to the model illustrated in Fig. 16. It this comprises the following components: a single diagonal concrete strut and two nodes. The numerical calculations demonstrated that the flow of compression stresses between nodes is similar to a “bottle” shape. This results from the different loading widths (distance between outer longitudinal reinforcement bars and contact plate width). In the numerical calculations, a flow of tension stresses was identified in the perpendicular direction to the compression flow, and this should be taken into account in the failure criterion of the concrete strut. However, as stated in Schlaich et al. [13], it can be assumed that the concrete strut is safe if the failure criterion of the nodes is satisfied. In addition, in the present study, the edge distances are not considered to affect the joint. Consequently, the nodes are the most relevant components of the proposed model. The identified nodes are of the following type: N1 is CTT, as two ties converge to the node; N2 is CCC, as only compression struts converge to the node. Finally, it should be stated that the horizontal reinforcement ties are considered as a component of the complete joint and not as part of the concrete panel.

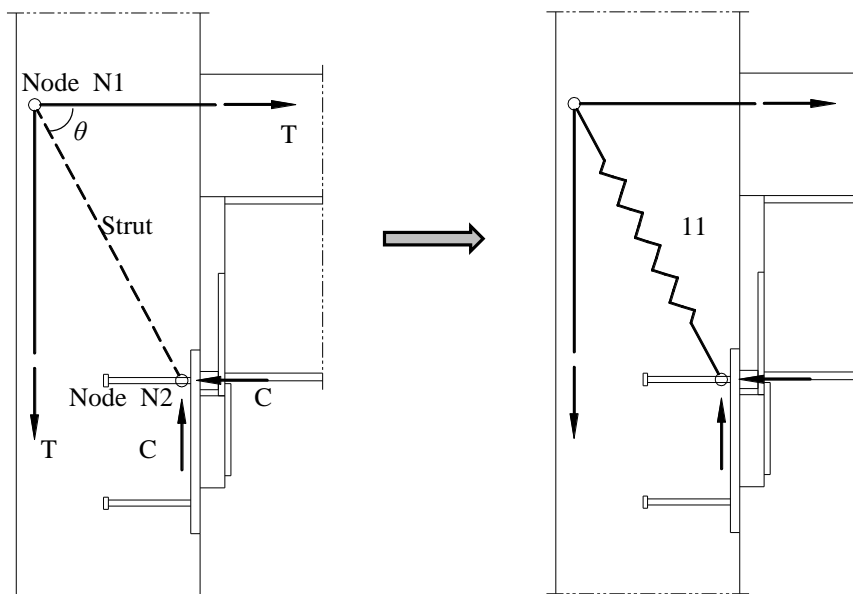


Fig. 16: Model proposed for the Concrete panel component

Thus, the following assumptions were considered in the concrete panel model:

- Components: Single diagonal concrete strut (bottle shape) and two nodes (one type CTT and one type CCC);
- Failure is governed by the nodal regions, and is disregarded within the strut;
- The flow of stresses through the wall to supports are not considered as part of the concrete panel and therefore not analyzed;
- Ties (longitudinal reinforcement) are components considered in the analysis of the complete joint and therefore are neglected for the concrete panel behavior;

- The deformation of the diagonal concrete strut is assumed to contribute to the global response of the joint.

#### 4.4.2 Characterization of the components and determination of the concrete panel properties

In terms of resistance, the model is characterized by the resistance of the nodes at the ends of the diagonal strut. Accordingly, the maximum admissible stresses and the geometry of these nodes define the concrete panel load capacity. The resistance of the nodes is obtained as follows.

##### a) Node N1 (type CTT)

The geometry of the node is defined in one direction by the bend radius of the longitudinal reinforcement and by the strut angle, as illustrated in Fig. 17 with the dimension  $a$ . In the other direction (along the width of the wall), it was observed that the stress distribution is non-uniform; as illustrated in Fig. 18a. Hence, as the analytical approach assumes that the stresses are constant within the dimension  $b_{rb}$  (distance between the outer longitudinal reinforcement bars), an effective width ( $b_{eff,rb}$ ) was proposed. It was calibrated on the basis of a parametric study and the numerical model shown in Fig. 18b. The diameter of the reinforcement bar ( $d_{rb}$ ), the spacing of bars ( $s_{rb}$ ) and the strut angle ( $\theta$ ) were identified as the main parameters influencing the effective width ( $b_{eff,rb}$ ). The influence of the wall edges was disregarded.

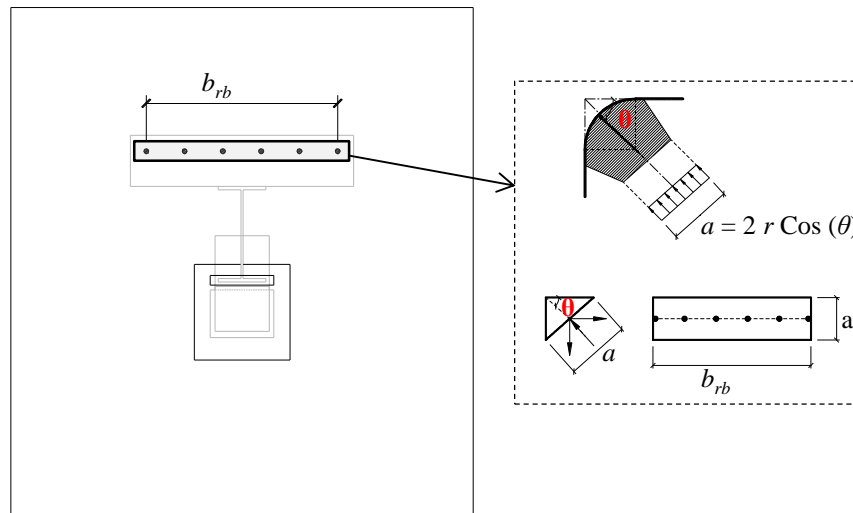


Fig. 17: Definition of the width of the node N1



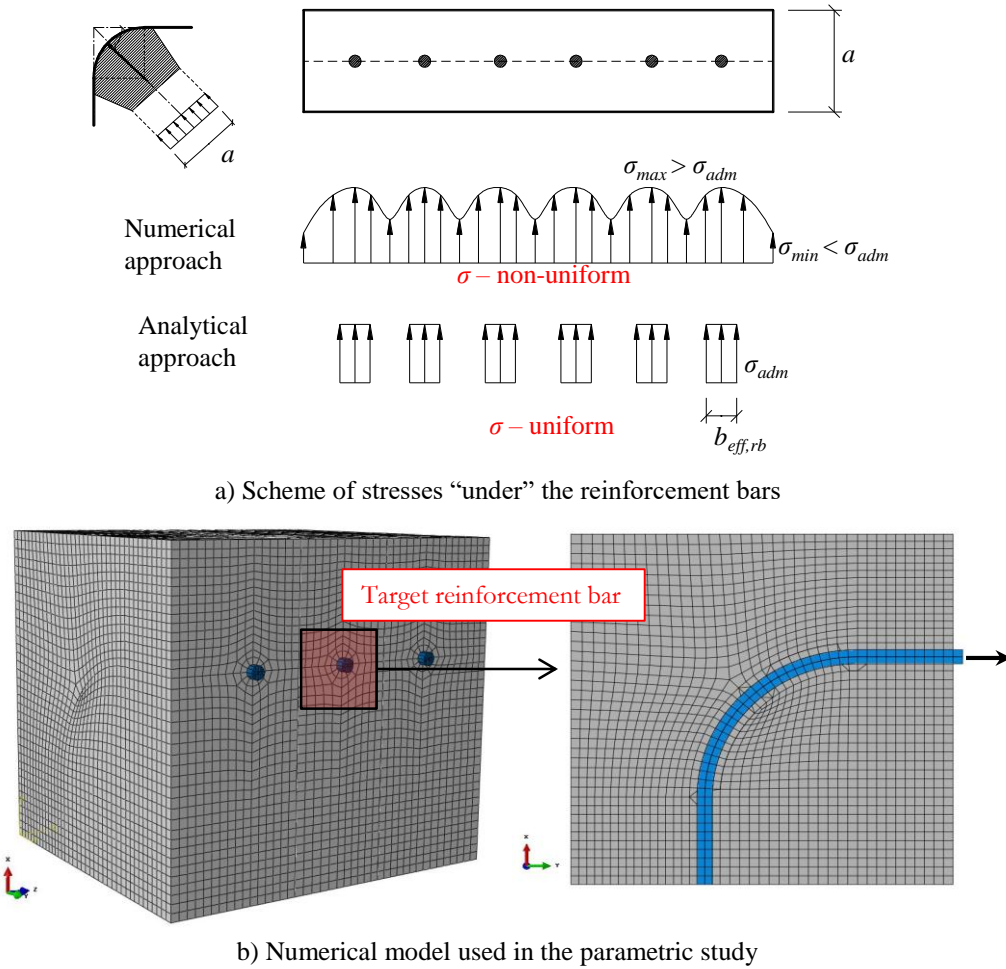


Fig. 18: Approach to derive the effective width under each reinforcement bar subjected to constant admissible compression stresses in a CTT node with bent reinforcement bars

Based on the numerical simulations [16], the node resistance is obtained as follows:

$$\begin{cases} s_{rb} \geq 80 \text{ mm}: b_{eff,rb} = 2.62 d_{rb}^{0.96} (\text{Cos } \theta)^{-1.05} \\ s_{rb} < 80 \text{ mm}: b_{eff,rb} = 2.62 d_{rb}^{0.96} (\text{Cos } \theta)^{-1.05} \left(\frac{s_{rb}}{80}\right)^{0.61} \end{cases} \quad (22)$$

$$A_{N1} = b_{eff,rb} 2r \text{Cos}(\theta) \quad (23)$$

$$F_{r,N1} = A_{N1} 0.75 v f_{cd} \quad (24)$$

where  $A_{N1}$  is the cross-section area of the diagonal concrete strut at node N1 where the admissible stresses have to be verified,  $b_{eff,rb}$  effective width of the concrete contributing to the node resistance,  $r$  is the bend radius of the longitudinal reinforcement bars and  $\theta$  is the angle of the concrete strut with the horizontal direction.

#### b) Node N2 (type CCC)

The geometry of the node, on the concrete strut edge, is defined by the projection of the dimensions of the equivalent rigid plate, representing the anchor plate subjected to

compression, in the direction of the concrete strut. Fig. 19 illustrates the geometry and the dimensions of this node, leading to:

$$A_{N2} = \frac{l_{eff}}{\cos(\theta)} b_{eff} \quad (25)$$

where  $A_{N2}$  is the cross-section area of the diagonal concrete strut at node N2 where the admissible stresses have to be verified and  $l_{eff}$  and  $b_{eff}$  are the dimensions of the equivalent rigid plate [16].

Considering the admissible stresses and the node dimensions, the resistance of the node is obtained [16].

$$F_{r,N2} = A_{N2} 3v f_{cd} \quad (26)$$

$f_{cd}$  is the concrete design strength and  $v$  is a factor related to the concrete characteristic compressive strength ( $f_{ck}$ ).

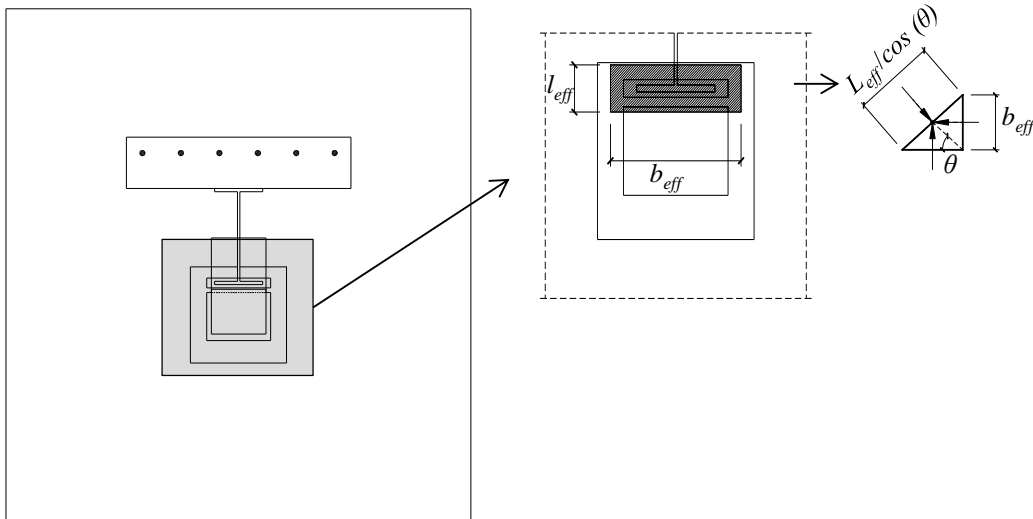


Fig. 19: Definition of the dimensions of node N2

### c) Concrete panel properties

The resistance of the concrete panel is given by the minimum resistance of the two nodes, N1 and N2, eq. (27) [16]. Note that the resistance is projected in the horizontal direction. It should be noted that for equilibrium in node N1, the vertical component of the load in the diagonal strut has to be equilibrated by the vertical reinforcement in the wall. The design of this reinforcement is not analyzed in the present study.

$$F_{C-T,CP} = \text{Min}(F_{r,N1}; F_{r,N2}) \text{Cos}(\theta) \quad (27)$$

In terms of deformation, the problem is more complex as the strain field within the diagonal strut is highly variable. However, as the deformation pattern of the concrete panel is not very sensitive to geometric variations [16], a mathematical expression (eq. (28)) was fitted to the numerical force-deformation curve. Thus, the horizontal projection of the deformation of the diagonal strut is obtained as a function of the horizontal component of the load on the strut. In eq. (28), the load ( $F_{C-T,CP}$ ) is introduced in kN and the deformation is obtained in mm.

$$d_{h,CP} = (6.48E^{-8} F_{C-T,CP}^2 + 7.47E^{-5} F_{C-T,CP}) \text{Cos} \theta \quad (28)$$

#### 4.4.3 Application and validation of the model

In order to assess the quality of the analytical model proposed for the concrete panel, it was applied and compared to the numerical results [16]. Table 9 shows good agreement between these results, both in terms of failure mode (upper node in all cases) and resistance, except for thinner walls (150 mm) where the ratio is below 0.6. Plotting the resistance ratio as a function of the angle of the strut ( $\theta$ ), as shown in Fig. 20, it can be observed that the analytical model loses accuracy for angles above 70°, becoming too conservative. For these cases, a different STM model should be considered, e.g. adopting two diagonal springs with height equal to half of the lever arm. However, this was not pursued in the present work.

Table 9: Ratio between  $F_{CP,An}/F_{CP,Num}$

<b>Parameter Thickness of wall</b>	<b>Ratio [<math>F_{CP,An}/F_{CP,Num}</math>]</b>	<b>Parameter Height of composite beam</b>	<b>Ratio [<math>F_{CP,An}/F_{CP,Num}</math>]</b>	<b>Parameter Bend radius of longitudinal reinforcement</b>	<b>Ratio [<math>F_{CP,An}/F_{CP,Num}</math>]</b>
JL-T150	0.588	JL-H226	0.998	JL-R80	0.850
JL-T200	0.855	JL-H416 [Ref]*	0.997	JL-R120	0.974
JL-T250	0.965	JL-H620	0.826	JL-R160 [Ref]*	0.997
JL-T300 [Ref]*	0.997				
JL-T350	0.977				
JL-T400	0.951				

\*Ref – is the reference model which uses the same geometrical properties as in the tests performed in [15]

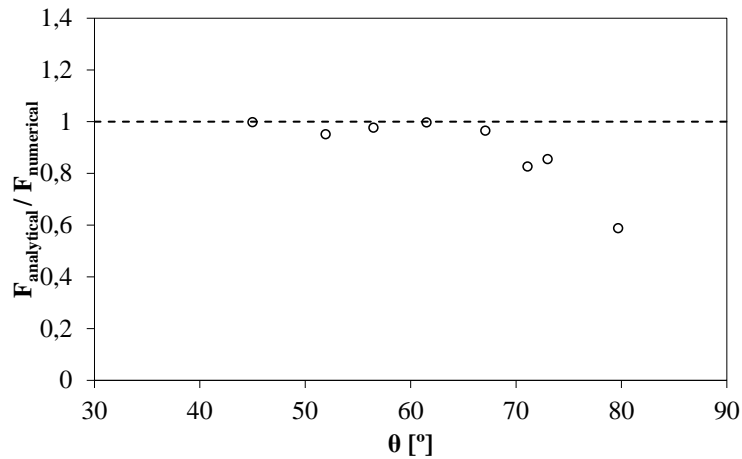


Fig. 20: Influence of the strut angle ( $\theta$ ) on the analytical prediction

#### 4.5 Joint mechanical model and assembly of joint components

##### 4.5.1 Idealized model

The joint components activated in the composite beam to reinforced concrete wall joint, subjected to hogging bending moment, were identified in Table 5. Accordingly, a representative spring and rigid link model was idealized and it is illustrated in Fig. 21a. Two vertical rigid bars separate three groups of springs. The rigid bars avoid the interplay between tension and compression components, simplifying the joint assembly. Another simplification was introduced by considering a single horizontal spring to represent the concrete panel. In what concerns the tension springs, it was assumed that slip and the longitudinal reinforcement are at the same level although slip is observed at the steel beam – concrete slab interface. Finally, concerning the anchor plate, an equivalent translational spring  $(5-10)_{\text{eq}}$  was considered, leading to the simpler joint model of Fig. 21b.

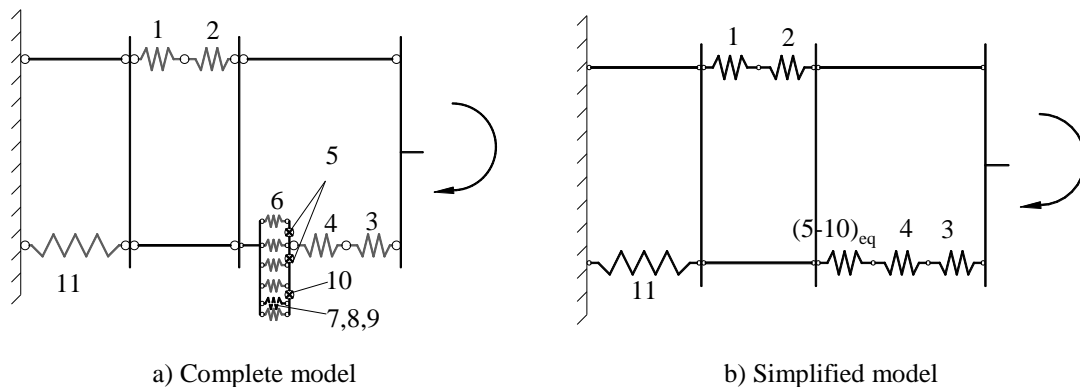


Fig. 21: Joint component model for the composite beam to reinforced concrete wall joint

#### 4.5.2 Joint assembly and determination of the joint properties

For the joint under hogging bending moment, the assembly procedure is based on the mechanical model depicted in Fig. 21b. The determination of the joint properties under bending moment was performed using two different approaches: “optimized” and “simplified”. EC4 model [4]). In the first case, the longitudinal steel reinforcement bar in slab follows the ECCS recommendations [24], while the slip of the composite beam and the anchor plate components consider the “sophisticated” models described before. For the second approach, the longitudinal steel reinforcement bar in slab follows the EC4 model [4], while the anchor plate components consider the “simplified” models.

##### a) “Optimized” model

The mechanical model represented in Fig. 21b presents only one row of components in tension and another in compression. This leads to a simple assembly procedure, as no distribution of load is required amongst rows, as in steel/composite joint with two or more tension rows. Thus, the first step is the assembly of the components per row. Equivalent springs are defined per row, as represented in Fig. 22. The determination of their properties takes into consideration the relative position of the components: acting in series or in parallel [16], leading to eqs. (29) and (30), for resistance ( $F_{eq,t}$  and  $F_{eq,c}$ ) and deformation ( $\Delta_{eq,t}$  and  $\Delta_{eq,c}$ ), respectively.

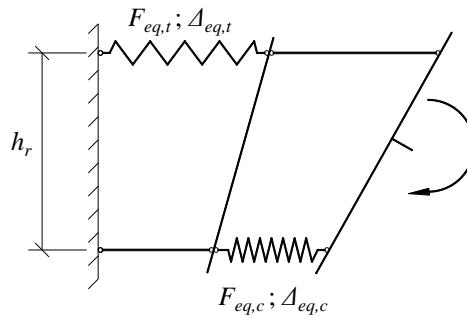


Fig. 22: Simplified joint model with assembly of components per row

$$F_{eq} = \text{Min}\{F_i \text{ to } F_n\} \quad (29)$$

$$\Delta_{eq} = \sum_{i=1}^n \Delta_i \quad (30)$$

where the index  $i$  represents all relevant components either in tension or in compression, depending on the row under consideration.

In order to determine the joint properties ( $M_j$ ,  $\Phi_j$ ), it is necessary to define the lever arm  $h_r$ . According to the joint configuration, it was assumed that the lever arm is the distance between the centroid of the longitudinal steel reinforcement bar and the mid

thickness of bottom flange of the steel beam. The centroid of steel contact plate is aligned with this reference point of the steel beam. Accordingly, the joint properties are obtained as follows [16]:

$$M_j = \text{Min}\{F_{eq,t}; F_{eq,c}; F_{CP}\} h_r \quad (31)$$

$$\Phi_j = \frac{\Delta_{eq,t} + \Delta_{eq,c} + \Delta_{CP}}{h_r} \quad (32)$$

where  $F_{eq,t}$  and  $F_{eq,c}$  are the equivalent resistance of the tension and compression rows, respectively, determined using eq. (29);  $\Delta_{eq,t}$  and  $\Delta_{eq,c}$  are the equivalent deformation of the tension and compression rows, respectively, determined using eq. (30), FCP is the concrete panel resistance, (eq. (27)) and DCP is the deformation of the concrete panel (eq. (28)).

#### b) “Simplified” model

In what concerns to the model assembly, the main difference lies in the deformation model which consists in the calculation of the joint initial rotational stiffness. Using the stiffness coefficients of the joint components, the joint rotational stiffness may be determined as expressed in eq. (33) as prescribed in [6]. For the concrete panel, no stiffness coefficient was derived though, as the contribution of this component is considerably smaller. Thus, as for two of the compression components, this component may be assumed as infinite rigid.

$$S_{j,ini} = \frac{Eh_r^2}{\left(\frac{1}{k_{eq,t}} + \frac{1}{k_{eq,c}}\right)} \quad (33)$$

$k_{eq,t}$  and  $k_{eq,c}$  are the equivalent stiffness coefficient of the tension and compression components, respectively.

In the case of structural non-linear analysis, the joint characterization requires the determination of its ultimate rotation capacity. This property is strongly dependent on the limiting component. As observed in the joint tests [15], this component is the longitudinal steel reinforcement bar. In the code, no estimation of the ultimate deformation capacity of this component is provided. The ECCS publication [24] proposes a model to evaluate this parameter. This model is suggested for evaluation of the joint rotation capacity. As conservative approach, the joint ultimate rotation capacity may be determined using only the ultimate deformation capacity of the longitudinal steel reinforcement bar in the slab, and neglecting the contribution of the other joint components [16]. Thus, in eq. (34), the component ultimate deformation ( $\Delta_{sru}$ ) should be obtained using the appropriate equation given before.

$$\Phi_{j,u} = \frac{\Delta_{sru}}{h_r} \quad (34)$$

The complete moment-rotation curve is obtained using the same principles as in Eurocode 3 Part1-8 [6] for steel joints. The modified ( $S_j$ ) stiffness was determined using the appropriate joint stiffness modification coefficient  $\eta$ , as expressed in eq. (35). The non-linear moment-rotation curve was defined using the joint stiffness expression prescribed by Eurocode 3 Part1-8 [6], as reproduced in eq. (36). In this expression, the stiffness ratio ( $\mu$ ) is constant and equal to 1 up to  $2/3$  of  $M_{j,Rd}$ , after a non-linear range is defined up to  $M_{j,Rd}$ , as expressed in eq. (37).

$$S_j = \frac{S_{j,ini}}{\eta} \quad (35)$$

$$S_j = \frac{Eh_r^2}{\mu \sum_i \frac{1}{k_i}} \quad (36)$$

With

$$\begin{cases} \text{if } M_{j,Ed} \leq \frac{2}{3} M_{j,Rd}: \mu=1 \\ \text{if } \frac{2}{3} M_{j,Rd} < M_{j,Ed} \leq M_{j,Rd}: \mu = \left( \frac{1.5 M_{j,Ed}}{M_{j,Rd}} \right)^\Psi \end{cases} \quad (37)$$

The coefficient  $\Psi$  is assumed equal 1.7 as recommend in Eurocode 4 [4] for a contact plate joint. Values for the rotational stiffness modification coefficient ( $\eta$ ) are provided in Eurocode 3 Part1-8 [6]. These vary according to the joint configuration. In the case of beam-to-column joints the value of 2 is proposed. In the case of composite beam to reinforced concrete walls, no information is available and therefore the use of the value for steel and composite joints is suggested.

#### 4.6 Validation of the model

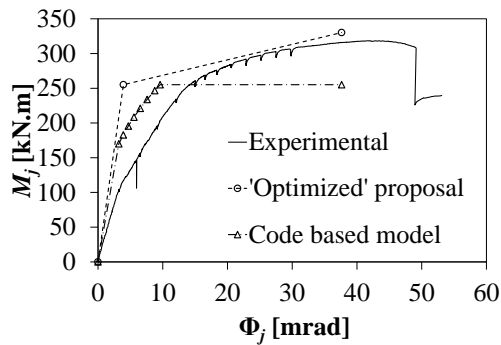
The application of the model is shown in Fig. 23. The joint bending moment to joint rotation curves compare analytical models and experimental tests. The quality of the model varies with parameter under analysis and with the type of model, “optimized” or code based. For the resistance, the approximation of the “optimized model” is excellent. The code model limits the governing component, the longitudinal steel reinforcement bar, to its yield capacity therefore, the lower resistance obtained with this model was expected. In terms of initial stiffness, the quality of the models is reversed. For this parameter, the code model provides a better approximation, being very close to the experimental results. In what concerns the “optimized” model, it was seen that the initial stiffness required improvement. A stiffer response was observed which may be attributed to the fact that the “optimized” model neglects discontinuity in the wall-slab interface. Because these members are concreted in different stages, the small bond developed between these members is rapidly exceeded. Consequently, an initial “crack” between wall and slab may be assumed from the beginning of loading and therefore the

joint is a more flexible than if full continuity existed between these members. As the code base model provided a good approximation for this parameter. It was decided to propose a modification to the joint component model described above. In this way, the initial stiffness is determined using same elongation length as used in the code based model:  $3.6h$ . See Fig. 15 for definition of the dimension  $h$ . Subsequently, the model to determine the ultimate deformation was also modified introducing the previous consideration. In Table 10 is summarized the modifications proposed in [16] for the “optimized” model of the longitudinal steel reinforcement bar in the slab component. Though, it should be noted that if wall and slab are concreted at the same time, the initial proposal for the “optimized” model should be more accurate and therefore used instead of the proposed modification. In what respects to the ultimate rotation, the “optimized” model is conservative though, also the analytical model to determine the ultimate deformation of the longitudinal steel reinforcement bar should be affected by the wall-slab interface behavior. The code based model is absent in what concerns this parameter. The limit of the represented plateau was assumed equal to the ultimate joint rotation determined with the “optimized” model.

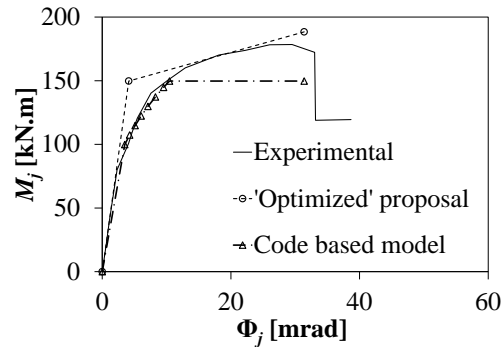
According to the results presented Fig. 23, both models present a good approximation of the joint behavior and therefore, are suitable for application.

Table 10: Proposed modifications for the “optimized” model of the longitudinal steel reinforcement in slab component

<b>Elongation length</b>	$3.6h$
<b>Ultimate deformation</b>	$\rho < 0.8\%: \Delta_{sru} = 3.6h\varepsilon_{sr\mu}$ $\rho \geq 0.8\% \text{ and } a < L_t: \Delta_{sru} = 3.6h\varepsilon_{sr\mu}$ $\rho \geq 0.8\% \text{ and } a > L_t: \Delta_{sru} = 3.6h\varepsilon_{sr\mu} + (a - 3.6h)\varepsilon_{sr\mu}$

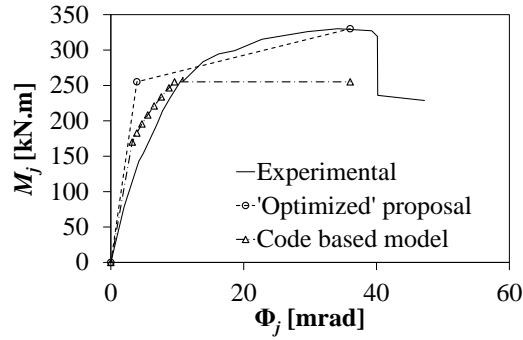


a) SP13



b) SP14





c) SP15

Fig. 23: Joint bending moment to joint rotation curve ( $M_j-\Phi_j$ ) comparing modification on the “Optimized” model with experimental tests and code based model results

## 5. Design procedure

The design procedure to determine the joint properties is summarized here below (Fig. 24). The range of validity of the proposed procedure is limited to joint configurations with only one row of longitudinal reinforcement in tension. In the case of more than one row in tension, the distribution of forces amongst tension rows and the assembly procedure should be similar to that prescribed by the [6] for steel joints. However, it has not yet been validated.

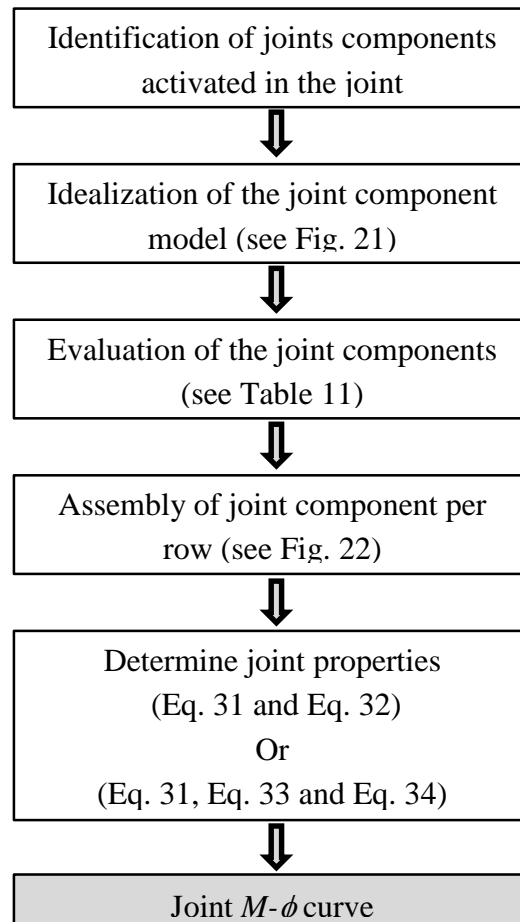


Fig. 24: Composite beam to reinforced concrete wall joint design procedure

Table 11: Summary of the design expressions to determine the joint components behavior

Component	Property	Expressions
Longitudinal reinforcement	Resistance [16], [24]	$F_{sr} = \sigma_{sr} A_{sr}$ with $\sigma_{sr1,d,SLAB} = \frac{\sigma_{sr1,SLAB}}{\gamma_S} = \frac{f_{ctm,SLAB} \cdot k_c}{\gamma_S \cdot \rho} \left[ 1 + \rho \frac{E_s}{E_c} \right]$ $\sigma_{sr1,d,WALL} = \frac{\sigma_{sr1,WALL}}{\gamma_S} = \frac{f_{ctm,WALL} \cdot k_c}{\gamma_S \cdot \rho} \left[ 1 + \rho \frac{E_s}{E_c} \right]$ $\sigma_{srn,d,SL} = 1.3 \cdot \sigma_{sr1,d,SL}$ $\sigma_{srn,d,WA} = 1.3 \cdot \sigma_{sr1,d,WA}$
	Stiffness [16], [24]	$\Delta \leq \Delta_{sry}: \quad \Delta = \varepsilon_{WA} h + \varepsilon_{SL} L_t$ $\varepsilon_{sr1,SL} = \frac{\sigma_{sr1,d,SL}}{E_s} - \Delta \varepsilon_{sr,SL} \quad \varepsilon_{sr1,WA} = \frac{\sigma_{sr1,d,WA}}{E_s} - \Delta \varepsilon_{sr,WA}$ $\Delta \varepsilon_{sr,SL} = \frac{f_{ctm,SL} \cdot k_c}{\gamma_S \cdot E_s \cdot \rho} \quad \Delta \varepsilon_{sr,WA} = \frac{f_{ctm,WA} \cdot k_c}{\gamma_S \cdot E_s \cdot \rho}$ $\varepsilon_{srn,SL} = \varepsilon_{sr1,SL} + \Delta \varepsilon_{sr,SL} \quad \varepsilon_{srn,WA} = \varepsilon_{sr1,WA} + \Delta \varepsilon_{sr,WA}$ $\varepsilon_{smy,SL} = \frac{f_{syk,d} - \sigma_{srn,d,SL}}{E_s} + \varepsilon_{sr1,SL} + \Delta \varepsilon_{sr,SL}$ $\varepsilon_{smy,WA} = \frac{f_{syk,d} - \sigma_{srn,d,WA}}{E_s} + \varepsilon_{sr1,WA} + \Delta \varepsilon_{sr,WA}$ $\varepsilon_{smu,SL} = \varepsilon_{sy} - \beta_t \Delta \varepsilon_{sr,SL} + \delta \left( 1 - \frac{\sigma_{sr1,d,SL}}{f_{syk,d}} \right) (\varepsilon_{su} - \varepsilon_{sy})$ $\varepsilon_{smu,WA} = \varepsilon_{sy} - \beta_t \Delta \varepsilon_{sr,WA} + \delta \left( 1 - \frac{\sigma_{sr1,d,WA}}{f_{syk,d}} \right) (\varepsilon_{su} - \varepsilon_{sy})$ $\rho < 0.8\%: \quad \Delta_{su} = 2 \cdot L_t \cdot \min(\varepsilon_{smu,SL}, \varepsilon_{smu,WA})$ $\rho \geq 0.8\% \text{ and } a < L_t: \quad \Delta_{su} = \frac{h_c}{2} \cdot \varepsilon_{smu,WA} + L_t \cdot \varepsilon_{smu,SL}$ $\rho \geq 0.8\% \text{ and } a > L_t: \quad \Delta_{su} = \frac{h_c}{2} \cdot \varepsilon_{smu,WA} + L_t \cdot \varepsilon_{smu,SL} + (a - L_t) \cdot \varepsilon_{smy,SL}$
Slip of beam	Resistance [4]	Eq. 24 with $P_{RK} = \min \left( \frac{0.8 \cdot f_u \cdot \pi \cdot d^2}{\gamma_V \cdot 4}; \frac{0.29 \cdot \alpha \cdot d^2 \sqrt{f_{ck} \cdot E_{cm}}}{\gamma_V} \right)$
	Stiffness	Eq. 27
Beam web and flange	Resistance [6]	$M_{c,Rd} = \frac{W_{pl} \cdot f_{syk}}{\gamma_M}$ $F_{c,fb,Rd} = \frac{M_{c,Rd}}{(h_b - t_{fb})}$
	Stiffness	Assumed infinite (Rigid component)
Concrete panel	Resistance	Eq. 34
	Stiffness	Eq. 35
T-Stub	Resistance [16]	$F_{C,Rd} = \frac{f_{jd} \cdot A_{eff}}{\gamma_C}$ with $A_{eff} = \min(2c + b_{cp}; b_{ap}) \cdot (c' + l_{cp} + \min(c, e_{1,cp}))$
	Stiffness	Eq. 16

Steel contact plate	Resistance [4]	$F_{cp} = \frac{f_{y,cp} \cdot A_{eff,cp}}{\gamma_M}$
	Stiffness	Assumed infinite (Rigid component)

## 6. Parametric study

### 6.1 Introduction

The design methodology presented in the previous sections is able to predict with good level of accuracy the behavior of the steel-concrete composite beam to reinforced concrete wall joint subject to hogging moment. It highlights that various distinct failure modes may control its behavior. In particular, depending on the critical component, either a ductile or a brittle behavior may be observed. Hence according to the design principles of the Eurocodes, it is important to assess and provide guidance for achieving a ductile behavior, especially if a semi-continuous design approach is to be used.

Table 5 identified the relevant components in the selected joint. Given that the longitudinal steel reinforcement is the component that may provide a ductile behavior, while the components that depend on the concrete behavior are brittle, a parametric study was carried out to assess the behavior for a realistic range of geometries and material properties. Attention is mainly focused on the steel reinforcement and the concrete panel. The force in the reinforcement is a function of the steel grade and of the bars layout. The first aspect concerns the yield strength ( $f_{syk}$ ), the ratio between ultimate and yield strength ( $k$ ) and ductility ( $\varepsilon_{s,u}$ ). The number and the diameter of bars and the number of layers characterize the second aspect. In the analysis, three values of  $f_{syk}$ , four values of  $k$ , three  $\varepsilon_{s,u}$  values and four reinforcement layouts are considered.

The possibility of the development of strut and tie mechanisms in the concrete panel depends on the angle  $\theta$ . This geometrical quantity is calculated through the ratio between the sum of the beam depth and the slab thickness and the thickness of the wall. In the analysis, six beam profiles, four wall thickness  $t_{wall}$  and three slab thickness  $s_{slab}$  are considered. The concrete properties of the wall, i.e. the characteristic compressive cylinder ( $f_{ck,cyl}$ ) or cubic ( $f_{ck,cube}$ ) strength, and secant modulus of elasticity ( $E_{cm}$ ), affect as well the concrete panel behavior. In the analysis, five concrete grades are considered for the wall. In total, the parametric study comprised 51840 combinations. Table 11 summarizes the parameters considered for the sensitivity study.

Table 12: Summary of the parametric study

Element	Parameter	
Reinforcement	Yield strength	
	$f_{syk}$ [MPa]	400      500      600
	Coefficient $f_u/f_{syk}$	
	$k$ [-]	1.05      1.15      1.25      1.35

	Ductility					
	$\varepsilon_{s,u}$ [%]	25	50	75		
	Bar layout					
		Case A	Case B	Case C	Case D	
	N layers [-]	1	1	1	2	
	N bars [-]	6	6	6	6	
	Diameter bars [mm]	12	14	16	16	
Slab	Thickness					
	$t_{slab}$ [mm]	120	160	200		
Wall	Thickness					
	$t_{wall}$ [mm]	160	200	240	300	
	Concrete Grade					
	$f_{ck,cyl}$ [MPa]	20	30	40	50	60
	$f_{ck,cube}$ [MPa]	25	37	50	60	75
	$E_{cm}$ [GPa]	30	33	35	37	39
Beam	Profile					
	IPE 240	IPE 270	IPE 300	IPE 330	IPE 360	IPE 400

To consider the possibility of two concrete grades for wall and slab, a modification of the approach given in ECCS Publication n° 109 [24] for longitudinal reinforcement behavior is proposed. Partial factors for steel reinforcements ( $\gamma_s = 1.15$ ), for steel ( $\gamma_M = 1.0$ ), for concrete ( $\gamma_C = 1.5$ ) and for design shear resistance of a headed stud ( $\gamma_v = 1.25$ ) are taken into account. Table 11 synthesizes the used method in the parametric analysis for all components.

## 6.2 Results and discussion

Considering the simultaneous variation of all parameters, the most common failure type is the concrete panel (65.9%); only in 28.0% of the cases slab reinforcement failure occurred; in few cases (6.2%) failure depends on the behavior of beam. Fig. 25 summarizes these results.

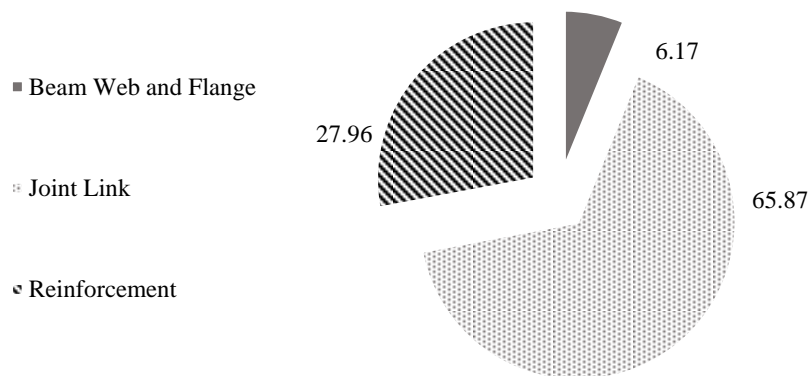


Fig. 25: Failure type

### 6.2.1 Influence of slab reinforcement

Fig. 25 illustrates the influence of the slab reinforcement. Firstly, increasing the reinforcement area, concrete panel failure grows significantly from 62.4% for Case A to 80.5% for Case C. Considering the reinforcement in two layers (Case D), brittle failures are 47.0%. Beam failure is only relevant in Case D (19.2%).

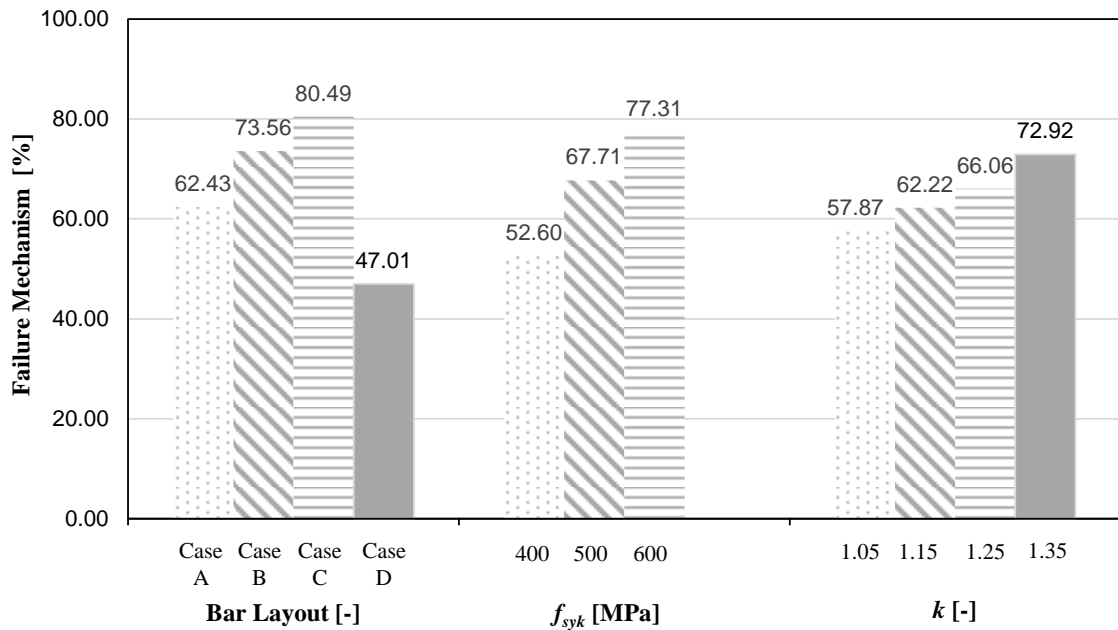


Fig. 26: Influence of slab reinforcement on brittle failure

As expected, one of the most influential parameter is the steel grade. Increasing the yield strength, the percentage of concrete panel failure increases from 52.6% to 77.3%. The variation of ductility of the rebars does not lead to changes in failure type distribution. Finally, increasing the ratio  $k$  leads to increased concrete panel failure from 57.9% to 72.9%.

### 6.2.2 Influence of angle $\theta$

Fig. 26 illustrates the influence of the angle  $\theta$ . The main parameter that affects the development of the failure mechanism is the wall thickness. Failure occurs in the concrete panel in 93.4% of cases for a thickness of 160 mm. This percentage drops to 76.0% for a thickness of 200 mm. Ductile failure only becomes the governing type of failure for a thickness of 300 mm (62.9%).

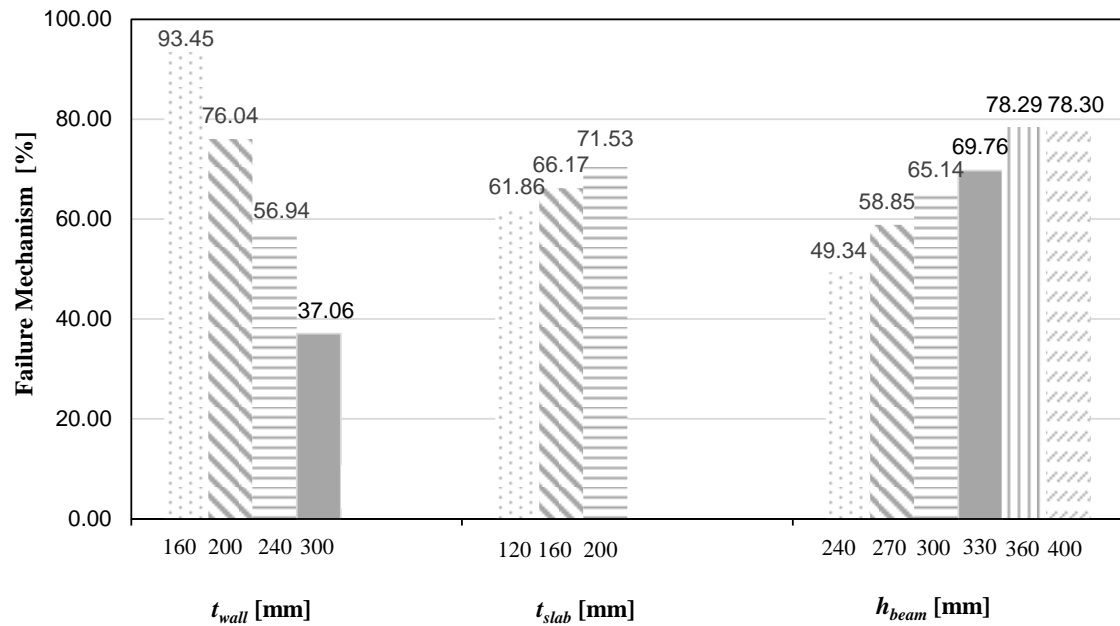


Fig. 27: Influence of angle  $\theta$

For the three values of the slab thickness considered (120 mm, 160 mm and 200 mm), failure happens in the concrete panel in most of the cases (variation between 61.9% and 71.5%). Beam failure does not vary appreciably (from 4.1% to 5.2%).

The depth of the beam determines a clear trend. For a depth of 240 mm, failure occurs in the concrete panel in about 50% of the cases, increasing to 78.3% for a beam depth of 400 mm. For low beam depths, beam failure is not negligible (22.8%), decreasing significantly for larger beam depths.

### 6.2.3 Influence of wall concrete grade

Fig. 28 shows the percentage of cases for each failure type. For concrete grade C20/25, concrete panel failure governs for almost all the cases (97.2%). This percentage drops approximately linearly to 36.9% for concrete C60/75.

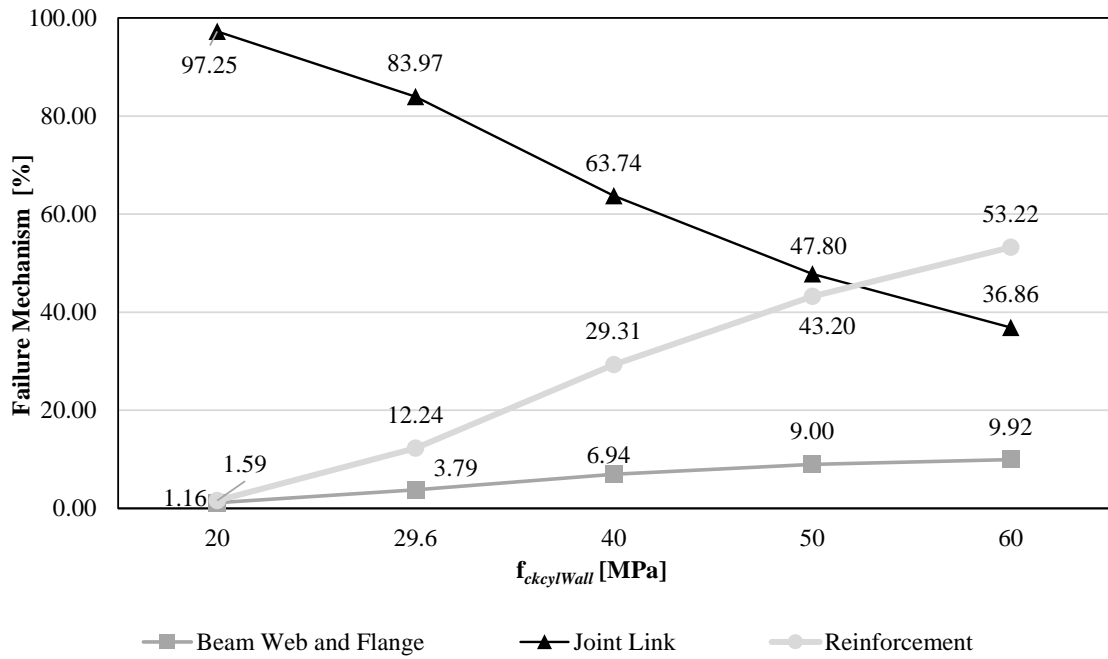


Fig. 28: Influence of wall concrete grade

#### 6.2.4 Combined influence of wall thickness and concrete grade

The combined influence of wall thickness and concrete grade is illustrated in Fig. 28. For a thickness of 160 mm, concrete panel failure governs for all types of concrete. This percentage drops from 100% (C20/25) to 81.9% (C60/75). The rate of decrease of concrete panel failure increases with increasing thickness, reaching only 3.0% for C60/75 and  $t_{wall} = 300$  mm.

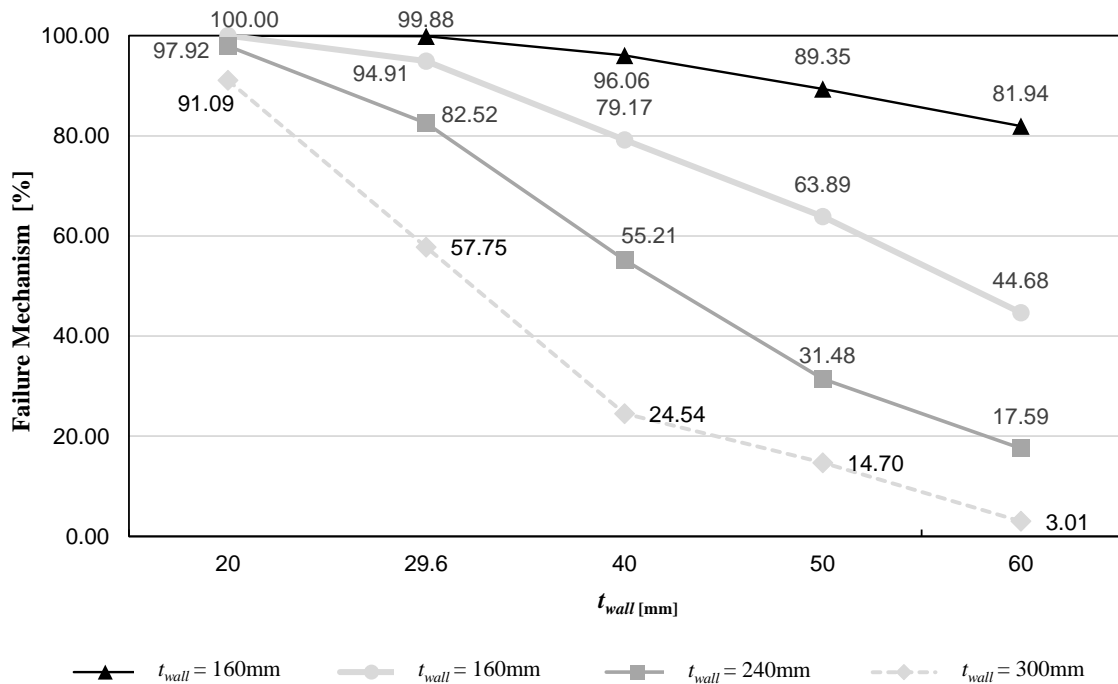


Fig. 29: Influence of wall concrete grade and wall thickness

## 6.2.5 Summary and pre design charts for ductile behavior

The sensitivity analysis shows the main parameters that affect the failure mode:

- yield strength: cases with brittle failure rises from 52.6% (for  $f_{syk} = 400$  MPa) to 77.3% (for  $f_{syk} = 600$  MPa);
- wall thickness: the concrete panel failure occurs in 93.4% of cases for a thickness of 160 mm and in 37.1% for a thickness of 300mm;
- total height of the composite beam: for the lowest value (360 mm) a ductile failure happens in 59.3% cases, while for the highest height, 19.7% of cases show this failure;
- concrete grade: for C20/25, there are 97.2% cases of brittle behavior, and this percentage drops to 36.9 % for concrete C60/75.

Though, these conclusions have to take into consideration that the joint model for the concrete panel has a limited accuracy related to the angle of the concrete strut. Outside of the range of concrete strut angles proposed, the model becomes conservative.

A pre design chart (Fig. 30) can be a useful tool in order to lead to a ductile failure. Here, the wall thickness (on the ordinate) is related to the concrete grade (on the abscissa). Separation curves between ductile (top-right) and brittle (bottom-left) failure can be built for nine steel grades (3  $f_{syk}$  and 3  $k$ ). To take into account the total height of the composite beam, three charts may be drawn: Fig. 30 represents the pre design chart for a total height between 360mm and 440mm; similar charts are available for other ranges of total height [37].

In Fig. 30, black lines refer to  $f_{syk} = 400$  MPa, dark grey to  $f_{syk} = 500$  MPa and light grey  $f_{syk} = 600$  MPa; solid lines refer to  $k = 1.05$ , dash lines to  $k = 1.15$ , long dash lines to  $k = 1.25$ , dash-dot-dot lines to  $k = 1.35$ . Curves stretches found for regression are shown dotted.

For example, for a total height of 390 mm, a wall thickness of 160 mm and a concrete characteristic compressive cylinder equal to 50 MPa, the steel yield strength that ensures a ductile behavior is equal to 400 MPa with a  $k = 1.05$ , according to Fig. 30.



Pre design chart for ductile behavior in case of total depth of the composite beam between 360 and 440 mm

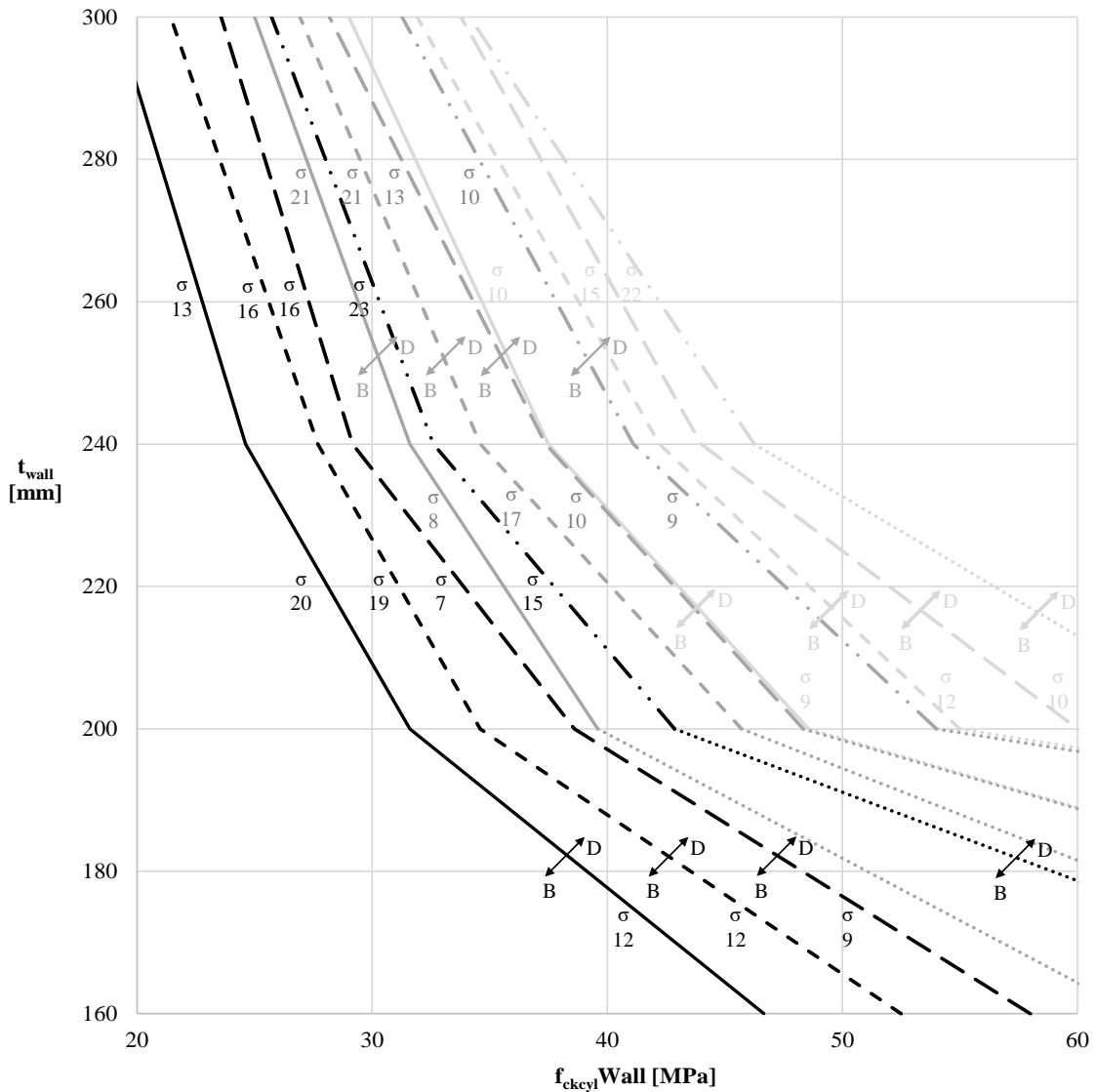


Fig. 30: Predesign chart for ductile behavior in case of total depth of the composite beam between 360 and 440 mm

## 6 - Conclusions

This paper presents a design model for moment resisting composite beam to reinforced concrete wall joints. It allows to determine the joint properties in terms of moment-rotation ( $M_j-\Phi_j$ ) curve. The basis of the presented study is the joint configuration developed within the research project InFaSo [15]. The objective to characterize the behavior of steel-to-concrete joints providing analytical tools, extending the component method, for a simple design was accomplished and may be summarized as follows:

- Identification of activated components

- Idealization of component model to reproduce the joint response
- Characterization of all activated components in terms of force-deformation curves
- Application and validation of joint model
- Parametric study

Tools for characterization of all activated components are presented in the paper. Though, the main emphasis has been given for those involving the concrete and therefore new components have been identified. The proposed models have been successfully validate against numerical and experimental data available. The integration of these components in the global joint has been later accomplished and the accuracy of the global model verified against experimental tests. The application this model to the test specimens of the experimental programme of the research project InFaSo [15] showed that the proposed models can provide an accurate characterization of the joint properties. Finally, the parametric study presented the application of the proposed model to a considerable number of cases exploiting the influence of different parameters related to material and geometrical properties. According to this study, as main outcome, the concrete panel appears as the component governing the joint response. Thus, to achieve a ductile behavior of the joint is essential to detail the concrete reinforcement in the concrete panel.

### **Acknowledgements**

Part of the work reported in this paper was granted by the Research Fund for Coal and Steel by the financed project N° RFSPR-2007-00051. The findings, observations and conclusions in this paper are, however, those of the writers.

### **References**

- [1] Stahlbau Magazine, 68(8), Ernst &Sohn, Berlin, 1999.
- [2] CEN, European Committee for Standardization (2004). Eurocode 2: Design of concrete structures – Part 1-1: General rules and rules for buildings. EN 1992-1-1; Brussels, Belgium, December 2004.
- [3] CEN, European Committee for Standardization (2005). Eurocode 3: Design of steel structures – Part 1-1: General rules and rules for buildings. EN 1993-1-1; Brussels, Belgium, May 2005.
- [4] CEN, European Committee for Standardization (2004). Eurocode 4: Design of composite steel and concrete structures – Part 1-1: General rules and rules for buildings. EN 1994-1-1; Brussels, Belgium, December 2004.
- [5] Stark, J.; Hordijk, D. A. Where structural steel and concrete meet. International Symposium on “Connections between steel and concrete”. University of Stuttgart, ed. Eligehausen R., Stuttgart, 2001, pp. 1-11, ISBN 2-912143-25-X.

- [6] CEN, European Committee for Standardization (2005) – “Eurocode 3: Design of steel structures – Part 1-8: Design of joints”, EN 1993-1-8, May 2005, Brussels, Belgium.
- [7] CEB. CEB Design Guide: Design of Fastenings in Concrete. Comité Euro-International du Béton, Lausanne, Suisse, 1997.
- [8] EOTA. Guideline for European Technical Approval of Anchors (metal anchors) for use in concrete. Part 1, 2 and 3 and annexes A, B, and C. Final Draft, EOTA; Brussels, February 1997.
- [9] ACI. ACI 318: ACI Standard 318. Building Code Requirements for Structural Concrete. American Concrete Institute; 2001.
- [10] fib, Federation International du Béton. fib Guide for the Design of fastenings in Concrete: Part 1: General, Part 2: Post-installed Anchors – Mechanical, Part 3: Post-installed Anchors – Bonded Anchors and Rebar Systems, Part 4: Headed Anchors, Part 5: Anchor Channels. Lausanne, 2007.
- [11] CEN, European Organization for Standardization. CEN Technical Specification (TS): Design of fastenings for use in concrete, Part 1: General, Part 2: Headed Fasteners, Part 3: Anchor Channels, Part 4: Post-installed Fasteners – Mechanical Systems, Part 5: Post-installed Fasteners – Chemical Systems. Brussels, 2007.
- [12] Eligehausen, R., Mallée, R., Silva, J. F., *Anchorage in Concrete Construction*, Ernst & Sohn, Berlin, 2006.
- [13] Schlaich, J., Schäfer, K., Jennewein, M., “Toward a Consistent Design of Structural Concrete”, *PCI Journal*, 32(3), pp. 74-150, 1987.
- [14] Wald, F., Sokol, Z., Steenhuis, C. M., Jaspert, J.-P. Component method for steel column bases. *Heron*, issue 1/2, 53 (3-20), 2008.
- [15] Kuhlmann, U, Eligehausen, R, Wald, F, da Silva, L, Hofmann, J, “New market chances for steel structures by innovative fastening solutions”, Final report of the RFCS project INFASO, project N° RFSPR-CT-2007-00051 (2014).
- [16] Henriques J. (2013). “Behaviour of joints: simple and efficient steel-to-concrete joints”, PhD Thesis, University of Coimbra, June, 2013.
- [17] Henriques, J, Simões da Silva, L, Valente, I. Numerical modeling of composite beam to reinforced concrete wall joints Part I: Calibration of joint components. *Engineering Structures*, 52, pp. 747-761, 2013.
- [18] Henriques, J, Simões da Silva, L, Valente, I. Numerical modeling of composite beam to reinforced concrete wall joints Part II: Global behavior. *Engineering Structures* 52, pp. 734-746, 2013.
- [19] Schäfer, M. “Zum Rotationsnachweis teiltragfähiger Verbundknoten in verschieblichen Verbundrahmen”, Doctoral Thesis, University of Stuttgart, July, 2005. (In German)
- [20] Zoetemeijer, P. A design method for tension side of statically«-loaded bolted beam-to-column joints. *Heron*, 20(1), pp. 1-59, 1974.

- [21] Jaspard, J.-P. Étude de la semi-rigidité des nœuds poutre-colonne et son influence sur la résistance des ossatures en acier. PhD Thesis (in French), University Liège, Liège, 1991.
- [22] Weynand, K., Jaspard, J.-P., Steenhuis, M. The Stiffness Model of Revised Annex J of Eurocode 3. in Bjorhovde R. Colson A. Zandonini R. (eds.) Connections in Steel Structures III, Pergamon, Oxford and New York, pp. 441-452, 1996.
- [23] Simões da Silva, L., Coelho, A. A ductility model for steel connections. *Journal of Constructional Steel Research*, vol. 41, N° 1, pp. 31-60, 2002.
- [24] European Convention for Constructional Steelwork – ECCS. *Design of Composite Joints for Buildings*. ECCS Publication n°109, Technical Committee 11 - Composite Structures, Belgium, 1999.
- [25] Schlaich, J., Schäfer, K. Design and detailing of structural concrete using strut-and-tie models. *The Structural Engineer*, 69(6), 1991.
- [26] Comité Euro-International du Béton - CEB. CEB-FIP Model Code 1990 : Design Code. Lausanne, 1993.
- [27] Narayanan, R S, Beeby, A. Designers' Guide to EN1992-1-1 and EN 1992-1-2. Eurocode 2: Design of concrete structures. General rules and rules for buildings and structural fire design. Series editor Haig Gulvanessian, Thomas Telford, London, 2005.
- [28] Federation International du Béton – fib. Practitioners' guide to finite element modelling of reinforced concrete structures. fib – Bulletin 45, Lausanne, 2008.
- [29] Guisse, S, Vandegans, D, Jaspard, J-P. Application of the component method to column bases: Experimentation and development of a mechanical model for characterization. Research Centre of the Belgian Metalworking Industry, MT195, Liège, 1996.
- [30] Wald, F, Sokol, Z, Steenhuis, M. Proposal of the Stiffness Design Model of the Column Bases. in Connections in Steel Structures III: Behaviour, Strength and Design, Proceedings of the Third International Workshop, pp. 237-249, Trento, 1996.
- [31] Weynand, K. Column bases in steel building frames. COST C1 - Semi-rigid behaviour of civil engineering structural connections, Luxembourg, 1999.
- [32] Steenhuis M, Wald F, Sokol Z, Stark J. Concrete in compression and base plate in bending. *Heron*, 53(1/2), pp. 51-68, Delft, 2008.
- [33] Demonceau, J. Steel and composite building frames: sway-response under conventional loading and development of membrane effects in beam further to an exceptional actions. PhD Thesis, University of Liège, Liège, 2008.
- [34] Anderson, D, Najafi, A A. Performance of Composite Connections: Major Axis End Plate Joints. *Journal of Constructional Steel Research*, vol. 31, pp. 31-57, 1994.
- [35] Aribert, J M. Influence of Slip on Joint Behaviour. in: Connections in Steel Structures III: Behaviour, Strength and Design, Third International Workshop, Trento, pp. 29-31, 1995.
- [36] Ahmed, B, Nethercot, D A. Prediction of Initial Stiffness and Available Rotation Capacity of Major Axis Composite Flush Endplate Connections. *Journal of Constructional Steel Research*, vol. 41, N° 1, pp. 31-60, 1997.

[37] Wald, F, Hofmann, J, Kuhlmann, U, Bečková, S, Gentili F, Gervásio H, Henriques J, Markus Krimpmann M, Ožbolt A, Ruopp J, Schwarz I, Sharma A, Simões da Silva, L, van Kann, J, “Design of steel-to-concrete joints, Design manual II”, RFCS project Valorisation of Knowledge for Innovative Fastening Solution between Steel and Concrete, project N° RFSPR-CT-2007-00051, 2014.